LBNL-40663
UC-410

ERNEST ORLANDO LAWRENCE BERKELEY NATIONAL LABORATORY

Interferometric Spectrometers

Anne Thorne and Malcolm Howells

Accelerator and Fusion Research Division

June 1997

To be published as
a chapter in
Techniques of Vacuum Ultraviolet Physics,
J.A. Samson and D.A. Ederer, eds.,
Academic Press,
Orlando, FL, 1997

REFERENCE COPY
Does Not
Circulate

Bldg. 50 Library - Ref.
Lawrence Berkeley National Laboratory

LBNL-40663
Copy 1

DISCLAIMER

This document was prepared as an account of work sponsored by the United States Government. While this document is believed to contain correct information, neither the United States Government nor any agency thereof, nor the Regents of the University of California, nor any of their employees, makes any warranty, express or implied, or assumes any legal responsibility for the accuracy, completeness, or usefulness of any information, apparatus, product, or process disclosed, or represents that its use would not infringe privately owned rights. Reference herein to any specific commercial product, process, or service by its trade name, trademark, manufacturer, or otherwise, does not necessarily constitute or imply its endorsement, recommendation, or favoring by the United States Government or any agency thereof, or the Regents of the University of California. The views and opinions of authors expressed herein do not necessarily state or reflect those of the United States Government or any agency thereof or the Regents of the University of California.

Interferometric Spectrometers

Anne Thorne
Imperial College of Science, Technology, and Medicine

Malcolm Howells
Lawrence Berkeley National Laboratory

To be published in Techniques of Vacuum Ultraviolet Physics
J.A. Samson and D.A. Ederer, editors, Academic Press, Orlando 1997

Chapter 6: Interferometric Spectrometers

1 Introduction to VUV interferometric spectrometers

In contrast to the well established field of grating spectrometry, interferometric spectrometry is a new technique for the VUV. There is no mention whatever of it in Samson's 1967 *Techniques of Vacuum Ultraviolet Spectroscopy*, although there is a precursor in the form of a short section on broadband interference filters. Of the two types of interferometric spectrometer described here, the Fabry-Perot was then widely used in the near UV, but Fourier transform spectrometry (FTS) was considered to be an infrared technique only. The situation now is quite different. Whereas the range of Fabry-Perot (F-P) interferometers has been somewhat extended, leading to limited use in the VUV, there has been a dramatic increase in both the wavelength range and the use of FTS. Operation in the visible and the near UV is now routine, and recent developments have shown it to be a viable technique for the VUV, with a current limit of about 140 nm. Moreover, instruments designed to work at still shorter wavelengths are under construction.

The fundamental differences between dispersive and interferometric spectrometry arise from the ways in which the spectral information is accessed. All spectrometers work by superposing a number of rays of varying phase, the number being $10^5 - 10^3$ for a grating, a few tens for a F-P interferometer and just two for the Michelson interferometer that is used for FTS. However, prisms and gratings distinguish different wavelengths by spreading them out spatially, using slits with their narrow dimension in the plane of dispersion, while interferometers work by imposing a wavelength-dependent spatial or temporal modulation on the signal and have axial symmetry. The well-known multiplex and throughput advantages of interferometric spectrometry, relevant in the IR but not necessarily in the VUV (see below), stem from this difference. As interferometric methods are somewhat unfamiliar to most VUV spectroscopists, we start with an initial overview of the instrumentation. More detail may be found in refs.[1, 2]

A Fabry-Perot interferometer consists of a pair of transmitting plates mounted parallel to one another with highly reflecting coatings on their facing surfaces. The incident light undergoes multiple reflections between these surfaces, with constructive interference giving a maximum of intensity for wavelengths λ satisfying

$$n\lambda = x = 2\mu t \cos\theta,$$

where n is an integer, t is the plate separation, μ is the refractive index of the medium between the plates and θ is the angle of incidence. The interference pattern consists of fringes of equal inclination (constant θ) localised at infinity. The traditional method of use was to fix μt and record the ring pattern photographically. Modern practice is to limit the angular spread ($\theta \sim 0$ – see the discussion on the throughput advantage below) and vary either μ (by changing gas pressure) or t, recording the interference signal photoelectrically. Whichever method is used, the narrow free spectral range of the F-P requires an auxiliary monochromator for order-sorting, as discussed in the next section.

FTS is usually based on a Michelson interferometer in which one (or sometimes both) of the mirrors is scanned to change the optical path difference x from zero up to some large positive or negative value L. As with the scanning F-P, the field of view is limited to the centre of the ring pattern, and the signal is recorded as a function of x. This signal, the 'interferogram', is the Fourier transform of the spectrum, and the latter is recovered, potentially with no ambiguity or 'order overlap', by performing the inverse FT. Variants of this basic instrument are described in sections 6.5–6.7.

FTS has largely superseded grating spectrometry in the infrared because of the high gains in signal-to-noise ratio arising from the multiplex and throughput advantages. In the visible and

UV, where the dominant noise is photon noise or light source fluctuations rather than detector noise, the multiplex advantage does not exist; indeed, there can actually be a multiplex disadvantage, as shown in section 6.3. The throughput advantage, however, applies to all interferometers in which the interfering beams are split by division of amplitude so that the interference pattern has circular symmetry. This is true for the F-P and for most of the FT interferometers described below. It is not true for division-of-wavefront interferometers, which require a slit geometry.

However, there are two other strong reasons for pursuing FTS into the VUV, one of which applies also to F-P spectrometry: the high spectral resolution that can be achieved. The resolution limit is determined by the maximum optical path difference between the interfering beams. In a grating spectrometer this is limited by the physical size of the grating, whereas in an interferometer it is determined by the length of the scan (FTS) or the plate separation and the effective number of multiple reflections (F-P), both of which can be made much larger than the width of a diffraction grating. The second reason, which applies only to FTS, is the wavelength advantage that arises from the strictly linear wavenumber scale derived from the sampling intervals of the interferogram. This makes accurate wavelength calibration possible from a very small number of reference lines (in principle, only one is needed).

One might add as further advantages of interferometric spectrometry the smaller size and greater flexibility of the instruments: high resolution can be achieved without the long focal length required in a dispersive instrument, and, whereas the performance of the latter is essentially fixed during its manufacture, that of F-P and FT spectrometers can be to a large extent determined by the method of use.

Before discussing these two types of interferometer in more detail, we return to the throughput advantage, which they hold in common. The optical path difference x between the beams reflected at two parallel surfaces separated by a distance t is given by

$$x = 2t\cos\theta \simeq 2t(1 - \theta^2/2) \tag{1}$$

where θ is the angle of incidence (Fig.6.1), which is always small enough to justify the expansion. As t is increased, the ring spacing for any one wavelength gets finer, and the maximum value of θ must be correspondingly reduced if it is to include only the 'central ring'. For the Michelson interferometer the criterion is that x should not vary by more than half a wavelength over the field of view at the maximum value of t (i.e., a phase change of π from centre to edge)[1, 2]. Since L, the maximum path difference, is $2t_{max}$, we have (for $\mu \sim 1$)

$$2t_{max}\theta^2/2 < \lambda/2 \text{ giving } \theta_m^2 = \lambda/L$$

By equation 6.16 the resolution limit in wavenumbers ($\sigma = 1/\lambda$) is related to L by $\delta\sigma = \delta\lambda/\lambda^2 = 1/2L$, so in terms of the resolving power, $\mathcal{R} = \lambda/\delta\lambda$, we have

$$\theta_m = \sqrt{2/\mathcal{R}} \tag{2}$$

This last relation holds also for the F-P interferometer. The angle $2\theta_m$ defines the field of view of the interferometer – i.e., the angle subtended by the (circular) entrance aperture at the collimating lens or mirror. The throughput is proportional to the corresponding solid angle Ω. Thus for an interferometric spectrometer the maximum allowable solid angle Ω_i is

$$\Omega_i = \pi\theta_m^2 = 2\pi/\mathcal{R} \tag{3}$$

To quantify the throughput advantage, we compare this with the field of view for a grating spectrometer. The resolution of the latter is assumed to be slit-limited rather than diffraction-limited, usually a valid assumption for high resolution spectrometry in the VUV. For a Littrow mounting with the grating at approximately 45° the angle subtended by the slit width is given

by $\theta_m \simeq 2/\mathcal{R}$. If β is the angle subtended by the slit height, the solid angle subtended by the slit area at the grating is given by $\Omega_g = 2\beta/\mathcal{R}$. The throughput advantage is then conventionally described by the ratio of the two solid angles for the same resolving power:

$$\Omega_i/\Omega_g = \pi/\beta \tag{4}$$

At moderate to high resolution slit curvature and other aberrations effectively limit β to less than 0.01 radians (a 1 cm slit for a 1 m spectrometer), so there is an apparent throughput advantage of nearly three orders of magnitude. In the VUV this gain is reduced for two reasons: the area of the interferometer beamsplitter is likely to be significantly smaller than that of the grating, and the number of reflections in the interferometer is inevitably greater than one. The real throughput ratio is likely to be below 100. Nevertheless, the gain in signal-to-noise ratio is still of the order of 10 for a photon noise limited system. If the dominant noise is from source fluctuations, the noise simply scales with the signal, and a larger throughput confers no advantage.

In summary, therefore, the unique advantages offered by interferometric over grating spectrometry in the VUV are the higher resolution and (in the case of FTS) the more accurate wavenumbers attainable. For resolving powers of order 100,000 that can be reached with either technique in the region down to 100 nm or so, interferometry offers a significant gain in signal-to-noise for photon-limited systems and also more compact and flexible instrumentation. As the attainable resolving power of grating spectrometers falls off almost linearly with wavelength (60,000 is the best value achieved at 20 nm), the resolution advantage is the primary reason for extending interferometric techniques into the grazing-incidence region (Section 7).

2 Fabry-Perot Interferometry

2.1 Instrument function and resolution

The Fabry-Perot interferometer consists of a pair of transmitting plates mounted with their facing surfaces accurately parallel, polished to a high degree of flatness, and coated with partially reflecting films. Figure 6.2 shows schematically the complex amplitudes of the reflected rays: each double pass introduces an additional factor $\rho^2 e^{i\phi}$, where ρ is the amplitude coefficient of reflection and ϕ is the phase increment, given by $\phi = 2\pi\sigma x = 4\pi\sigma t\cos\theta$. Summing these complex amplitudes and multiplying by the complex conjugate gives the well known Airy intensity distribution

$$I = I_o\left(\frac{T}{1-R}\right)^2 \frac{1}{1+f\sin^2(\phi/2)} \tag{5}$$

where I_o is the incident intensity, T and R are the transmissivity and reflectivity of the coatings ($R = \rho^2$) and $f = 4R/(1-R)^2$ [1, 2, 3]. This function is illustrated for two different values of R in Fig. 6.3. It has maxima whenever $\phi/2 = n\pi$ – i.e.,

$$I_{max} = I_oT^2/(1-R)^2 \text{ for } \sigma x = n \text{ or } 2t = n\lambda \tag{6}$$

The minima, $I_{min} = I_oT^2/(1+R)^2$, lie half way between the maxima.

The characteristics of the Airy distribution are as follows. First, for any given value of x the pattern is repeated at wavenumber intervals defined by unit change in the order n – i.e., $\Delta\sigma = 1/x$. The free spectral range is therefore given by

$$\text{FSR} = \Delta\sigma = \Delta\lambda/\lambda^2 = 1/2t \tag{7}$$

Second, the intensity does not fall to zero in the minima between the peaks. The contrast is given by

$$\text{Contrast} = I_{max}/I_{min} = (1+R)^2/(1-R)^2 \tag{8}$$

Third, the intensity transmitted by the interferometer at the peaks of the distribution is a fraction $T^2/(1-R)^2$ of the incident intensity (equation 6.6), and if the absorption in the coatings is negligible this is 100%. On the other hand if the absorption A is not negligible, then

$$\bar{I}_{max} = \left(\frac{1-R-A}{1-R}\right)^2 = \left(1-\frac{A}{1-R}\right)^2 \tag{9}$$

which drops rapidly with increasing A at the high values of R normally used. Finally, the resolving power of the interferometer is also strongly dependent on R. The Rayleigh criterion for resolution in its original form applies to a sinc^2 and not to an Airy instrumental function, but the criterion in a more generally applicable form states that two lines of equal intensity are just resolved if the minimum in the dip between them is 81% $(8/\pi^2)$ of the peak intensity. Applying this to the Airy distribution, making allowance for the finite contribution from the wing of each line to the peak intensity of the other, gives for the resolution limit $\delta\sigma$ in wavenumbers

$$\delta\sigma = \frac{2}{\pi\sqrt{f}}\Delta\sigma = \frac{1-R}{\pi\sqrt{R}}\Delta\sigma \tag{10}$$

The ratio of free spectral range to resolution limit measures the fine-ness, or 'finesse', of the fringes, N_r, given by

$$N_r = \pi\sqrt{R}/(1-R) \tag{11}$$

The suffix 'r' denotes reflection finesse; as pointed out below, there can be other contributions to the instrumental line width. By re-writing the free spectral range $\Delta\sigma = 1/2t$ (equation 6.7) in terms of the order number $n(= 2\sigma t)$ from equation 6.6, we obtain the resolving power as

$$\mathcal{R} = nN_r \tag{12}$$

By analogy with the similar expression for a grating, N_r can be interpreted as the effective number of interfering beams.

The resolution of the F-P does not match that expected from the reflectivity unless the reflecting surfaces are sufficiently flat. A bump of $\lambda/10$ changes the local path difference by $\lambda/5$, or a fifth of an order, and tends to spread the line correspondingly. This is taken into account by defining a plate finesse, N_p. Increasing N_r much above N_p does little for the resolution and loses light. A detailed treatment [2, 3] shows that the two should be approximately matched, and the effective finesse is then 0.6 of either.

2.2 Fabry-Perot spectrometry in the VUV

The problems of F-P interferometry in the VUV are apparent from the above discussion. Whereas almost loss-less dielectric coatings can be used in the visible and infrared, with N_r up to 50 or more, the reflectivities achieved with overcoated metal films in the VUV are unlikely to be better than about 75%, for which N_r is about 10, and even then their relatively large absorption makes for poor peak transmission (equation 6.9). If N_r is low, high resolution requires a high order number (equation 6.12) and a correspondingly low free spectral range, leading to more stringent requirements on the auxiliary monochromator. The fringe contrast is also low: for $R \simeq 70\%$ the contrast is less than 6. In addition the tolerances on surface flatness and parallelism of the plates scale directly with the wavelength. While it is possible to polish silica plates to reach a plate finesse of 30 at 200 nm, corresponding to 1/200 of a visible wavelength, it is much more difficult to obtain a good surface finish with the VUV-transmitting crystals that have to be used at shorter wavelengths. The problem of maintaining the plates parallel is usually solved by using a fixed spacer and enclosing the interferometer in a gas-tight box in which the

pressure can be varied to change the optical path between the plates. An interferometer of this type with a fixed spacer is usually known as a Fabry-Perot etalon.

The only systematic use of F-P spectrometry in the crystal transmission region of the VUV ($\lambda > 110$ nm)appears to have been by the group at Brest, who used silica F-P plates down to about 170 nm [4] and MgF_2 plates to reach 138 nm [5]. With the silica plates near 200 nm they were able to achieve reflection and plate finesses of close to 30, giving an overall finesse of about 17. At the shorter wavelengths ($\sim$ 150 nm) the poorer quality of the MgF_2 plates and the absorbance of the coatings combined to limit the overall finesse to about 4 or 5. The resolving powers depended on the choice of spacer and varied from nearly one million at 200 nm to about 100,000 at shorter wavelengths; it must be remembered that opting for high resolution when the finesse is low brings the penalty of a small free spectral range. The problems of realising better reflectance have been further discussed by this group [6]

At the other end of the VUV, in the soft X-ray region, there has been some work on high-reflection multilayer films that has resulted in the construction of F-P etalons with solid carbon spacers [7, 8, 9]. These devices have demonstrated reflection spectra (at grazing incidence) in the region around 0.15 nm and are scanned by changing the angle of incidence rather than the path difference between the 'plates'. The resolving power achieved is of order 100, with a finesse of about 2 to 3. It is not clear that the technique will have useful spectroscopic applications.

3 Fourier Transform Spectrometry: Principal Features

In this section the basic considerations and relations of FTS are presented for those unfamiliar with the technique. More background and detail can be found in the standard works on the subject, e.g., [10, 11, 12, 13], together with several comprehensive review-type articles [14, 15, 16, 17]; although none of this material covers UV, let alone VUV, FTS, the basic treatment is still valid. Apart from the practical implementation, which is discussed in the next section, the main difference between the IR and UV regions comes in the change from detector-limited noise, independent of the signal, to photon-limited noise, proportional to the square root of the signal. It is this change that loses the multiplex advantage and diminishes the importance of the throughput advantage.

3.1 The interferogram and the spectrum

The conventional instrument for FTS is a scanning Michelson interferometer in which the path difference x between the two interfering beams is varied up to some maximum value L. The scan can either be symmetric about zero path difference, or one side can be shorter than the other. The angular field of view is restricted as described in section 6.1 (equation 6.2) so that the detector records only the centre of the ring pattern at maximum path difference. The two-beam interference signal for a given wavenumber σ is then proportional to $(1 + \cos 2\pi\sigma x)$. If the spectral distribution from the source is described by some function $B(\sigma)$, the interference signals from all wavenumbers present are superposed to give $\int B(\sigma)(1 + \cos 2\pi\sigma x)\,d\sigma$.

This signal, recorded as a function of x, is the interferogram

$$I(x) = \int_0^\infty B(\sigma)\cos(2\pi\sigma x + \phi)\,d\sigma \tag{13}$$

In this expression the constant signal $\int B(\sigma)\,d\sigma$ has been subtracted off. The phase angle ϕ that has been added allows for the interferogram to be asymmetric about $x = 0$. There are two common causes of asymmetry: the sampling grid (see section 6.3.2 below) does not in general coincide exactly with $x = 0$, leading to $\phi = 2\pi\sigma\delta$ where δ is the offset; and the two interfering beams may traverse slightly different thicknesses of the beamsplitter material, leading to a

small additional path difference that is itself wavenumber dependent. Other small frequency-dependent contributions to ϕ may come from the electronic processing of the signal. ϕ is thus a function of σ but not of x. The asymmetry of the interferogram makes it necessary to use a complex Fourier transform to recover the complete spectral information in the form of the (complex) spectrum:

$$\mathrm{B}(\sigma) = \int_{-\infty}^{\infty} I(x) \exp(-2\pi i \sigma x)\, \mathrm{d}x = \mid \mathrm{B}(\sigma) \mid e^{i\phi(\sigma)} \tag{14}$$

Although it is possible just to take the spectrum as being represented by the modulus, a better procedure for several reasons [10, 14, 18] is to 'phase-correct': a low resolution phase spectrum $\phi(\sigma)$ is evaluated from a short central section of the interferogram and used to multiply the high resolution spectrum by $e^{-i\phi}$ so as to rotate the complex quantity $\mathrm{B}(\sigma)$ into the real plane.

There are two possibilities for varying the path difference x – either step-and-integrate or continuous scan. The latter is more common and is the method used in all the instruments referred to in section 6.4. If the rate of path change is v (twice the mirror velocity if only one mirror is moved), then $x = vt$ and the frequency f of the signal recorded by the detector for a wavenumber σ is given by $f = v\sigma$. Equation 6.13 can therefore be written as

$$I(t) = \int_{0}^{\infty} B(f) \cos(2\pi f t + \phi)\, \mathrm{d}f \tag{15}$$

The frequency f is just the optical frequency $\nu (= c/\lambda = c\sigma)$ downshifted by the factor v/c. v is normally chosen to put f in the audio range (say 1-20 kHz), avoiding any frequency ranges particularly sensitive to local noise.

3.2 Resolution and free spectral range

There are two important departures from the mathematically simple formulation of equation 6.14: the scan does not go out to $x = \infty$, and the signal is sampled and digitised at finite intervals rather than recorded in analogue form, so that the above integrals are actually sums. The consequence of the finite scan length L is to introduce an instrument function

$$I = I_o \frac{\sin 2\pi\sigma L}{2\pi\sigma L} \equiv \mathrm{sinc} 2\sigma L$$

The sinc function is illustrated in Fig. 6.4. The resolution limit is taken to be the distance from the central maximum to the first zero:

$$\text{resolution} \equiv \delta\sigma = 1/2L \text{ cm}^{-1} \tag{16}$$

This definition does not correspond exactly with the Rayleigh criterion, but it can be justified from the sampling theorem, as shown below. It is also close to the full width at half maximum, which is 1.2 $\delta\sigma$.

The sampling theorem states that in order to avoid ambiguity in the frequency domain a signal must be sampled at a frequency at least twice that of the highest frequency present in the spectrum – equivalent to sampling at intervals of not more than half the shortest wavelength: $\Delta x \leq \lambda_{min}/2 = 1/2\sigma_m$. The reason for this minimum sampling frequency (the Nyquist frequency) is apparent from the basic mathematics of the Fourier transform [11]. First, the FT of a single cosine wave of spatial frequency σ_o is a *pair* of delta functions, one at σ_o and the other at $-\sigma_o$. Thus the FT always generates both the actual spectrum and a mirror image of it at negative frequencies. Although the negative frequencies are physically unreal, they are important insofar as the mirror image affects the sampling requirements. Second, sampling the

interferogram is equivalent to multiplying it by a comb function of spacing Δx; in the spectral domain this represents convolution with a comb function of spacing $1/\Delta x$ – i.e., the spectrum is replicated at intervals of $1/\Delta x$, and the replication applies to the real spectrum *and* its mirror image, which together occupy a range $2\sigma_m$, as shown in Fig. 5a. It can be seen that the replications will begin to overlap unless the replication interval $1/\Delta x$ is at least equal to $2\sigma_m$. In the UV, however, much of the spectral range from 0 to σ_m is usually empty owing to the use of solar-blind detectors or optical filters. When the spectrum is contained within the bandwidth $\sigma_2 - \sigma_1$, as illustrated in Fig. 5b, the sampling interval can be increased up to $\Delta x = 1/2(\sigma_2 - \sigma_1)$ without overlapping. Considered the other way round, the free spectral range is determined by the sampling interval according to

$$\text{Free spectral range} \equiv \Delta\sigma = 1/(2\Delta x) \tag{17}$$

The high frequency spectral band in Fig. 5b is 'aliased' by undersampling into the empty lower frequency regions from 0 to $\Delta\sigma$ and $\Delta\sigma$ to $2\Delta\sigma$. It is often convenient to think of the spectrum as folded backwards and forwards at intervals of $\Delta\sigma = 1/2\Delta x$ as shown in Fig. 5c; each fold represents an alias, and the real spectrum in this case is in the third alias.

Two conditions must be met if undersampling is not to degrade the spectrum. First, some combination of source, detector and filter characteristics must ensure that the signal really is restricted to the free spectral range $\Delta\sigma$, and, second, a suitable electrical or digital bandpass filter should be used to prevent noise from other aliases from being folded back into the region of interest (see section 6.4).

It can be seen that the definition of resolution limit in equation 6.16 together with that of free spectral range in equation 6.17 ensures that the number of independent points N is the same in both the interferogram and the spectrum domains:

$$N = \Delta\sigma/\delta\sigma = 2L/(2\Delta x) = L/\Delta x \tag{18}$$

The spectrum sampled at intervals $\delta\sigma$ can be transformed back into the other domain to give the unaliased interferogram. Moreover, for an unaliased spectrum having a maximum frequency of σ_m, N is identical with the resolving power $\mathcal{R}$. If one is working in the nth alias the maximum wavenumber σ_{max} is $n\Delta\sigma$, so in general

$$\mathcal{R} = \sigma_{max}/\delta\sigma = nN \tag{19}$$

equivalent to equation 6.12 for the F-P and to the well known expression for a diffraction grating.

3.3 Wavenumber accuracy

It was stated in section 6.1 that high resolution and wavenumber accuracy are usually the most compelling reasons for using FTS rather than grating spectrometry in the VUV. The case for high resolution is obvious, for the resolution is determined only by the length L of the scan, and it should be possible to make this long enough to resolve the true line profiles of most laboratory sources. For atoms over the whole atomic mass range and for temperatures in the range 300-10000 K, the fractional Doppler widths $\delta\lambda_D/\lambda$, or $\delta\sigma_D/\sigma$, range approximately from 5×10^{-5} to 5×10^{-7}. If the instrumental width is required to be half the Doppler width, the corresponding resolving powers are in the range 40,000 to 4×10^6, and only the lower decade of this range is within the reach of even the largest grating spectrometer. With FTS a mirror displacement of 10 cm, giving $L = 20$ cm, corresponds to a resolving power of two million at 200 nm and nearly three million at 140 nm.

The wavenumber accuracy of FTS comes directly from the fact that a linear x-scale in the interferogram maps into a linear wavenumber scale in the spectrum, and in principle only

one reference wavenumber is needed to put this on an absolute scale. Usually, of course, several references are used to improve the accuracy, but it is not necessary to have them well distributed through the spectral range in the manner required for a grating spectrum. Since the x-scale is defined by the sampling intervals, which in practice are obtained from the interference fringes of a helium-neon laser following a path through the interferometer similar to that of the signal beam, it is tempting to use the laser wavenumber as the reference; this, however, can lead to errors of the order of $1/\mathcal{R}$ because the laser beam may not be strictly on axis ($\theta \neq 0$). Having established the absolute wavenumber scale, the next point to consider is the relative accuracy – that is, the uncertainty ϵ of determining the wavenumber of any given emission or absorption line. It has been shown [17, 19] that this can be expressed by

$$\epsilon = \frac{W}{\sqrt{n_p}(\mathrm{SNR})} \tag{20}$$

where W is the width of the line (in the same units as ϵ), n_p is the number of independent points across W, and SNR is the signal-to-noise ratio at the line peak. Thus high resolution (allowing Doppler-limited line widths) contributes directly to the wavenumber accuracy, provided it is not at the expense of poor SNR.

3.4 Signal-to-noise ratios

This last point leads naturally to a consideration of SNR in FT spectra, and in particular to the differences between grating spectrometry and FTS in this respect. The FT, being a linear process, simply adds the noise spectrum to the signal spectrum, and white noise (independent of frequency) therefore appears in the spectrum as a uniform level of noise, independent of the local signal. This is in contrast to a grating spectrum where, in the case of photon noise, the noise is proportional to the square root of the local signal. For FTS it can be shown (e.g., refs.[12, 15, 17] directly from the basic FT relations that

$$\left(\frac{\overline{s}}{n}\right)_s = \frac{1}{\sqrt{N}}\left(\frac{s_o}{n}\right)_i \tag{21}$$

where $\overline{s}$ is the mean signal in the spectrum, s_o is the signal at zero path difference in the interferogram, N is the number of independent points as given in equation 6.18, and the suffices s and i refer to the spectrum and the interferogram respectively. For an absorption spectrum, which is a quasi-continuum, the local signal is approximately the same as $\overline{s}$ except in deep absorption minima, and equation 6.21 is a reasonable representation of the SNR. In the case of emission spectra, most of the N spectral points have zero signal, and the signal at the peak of an emission line, s_p, can be very much greater than $\overline{s}$. Thus for an emission line we have

$$\left(\frac{s_p}{n}\right)_e = \left(\frac{s_p}{\overline{s}}\right)\left(\frac{\overline{s}}{n}\right)_s = \frac{1}{\alpha}\frac{1}{\sqrt{N}}\left(\frac{s_o}{n}\right)_i \tag{22}$$

where α is known as the filling factor and may be significantly less than 1% for even a fairly dense emission spectrum. One must be wary of concluding that the SNR is likely to be several hundred times better in an emission than in an absorption spectrum because the greater flux from a quasi-continuum should lead to a better SNR in the interferogram; if the system is photon-noise-limited, the net gain for an emission spectrum is likely to be about $\sqrt{\alpha}$ rather than α.

3.5 Comparison of FT and grating spectrometers

It is probably useful to summarise the important differences between these two types of spectrometer for operation in the VUV. Following directly from the last section, we start by comparing

SNRs for the same resolving power and the same light source, ignoring initially the throughput advantage of FTS. The direct comparison is most easily made for a quasi-continuous spectrum because the SNR is then the same for each of the N spectral elements for both instruments. In the same total time, a scanning grating records N independent spectral points, and a scanning interferometer records the same number of interferogram points. The signal falling on the interferometer detector (s_o in equations 6.21 and 6.22) is N times larger because it consists of all spectral elements, so for photon-noise-limits the interferometer has a gain of $\sqrt{N}$ in SNR. This factor is then lost in the Fourier transform, as shown in equation 6.21. Thus for an absorption spectrum the two instruments are equivalent – *if* the throughput gain of FTS is ignored. For an emission spectrum the filling factor enters into the equation. As a rough guide, FTS should give better SNRs for all lines down to an intensity of about $\sqrt{\alpha}$ of the stronger lines, while the SNR for the very weak lines should be better in a grating spectrum. However, the balance of SNR for both absorption and emission is shifted in favour of FTS by a factor that can realistically be put in the range 5-10 when the throughput advantage is taken into account.

There are two important exceptions to these conclusions. The first applies to a grating spectrometer equipped with an array detector. If all N spectral elements can be recorded simultaneously, the grating evidently gains a factor $\sqrt{N}$ in SNR for both absorption and emission spectra. Secondly, the comparison has assumed the noise to be predominantly photon noise; in the case of source noise, proportional to the signal rather than to its square root, the $\sqrt{N}$ (or $\sqrt{\alpha N}$) advantage to FTS from the larger signal falling on the detector is again lost.

Apart from SNRs there are two other obvious differences between FT and grating spectrometry that warrant a mention. First, an FT spectrometer cannot be used as a monochromator to produce radiation in a narrow wavelength band for some other experiment. It is true that the exit beam is differentially modulated, the modulation frequency being proportional to the wavenumber for any given scan velocity (equation 6.15); in principle this feature could be used to select a given band, but this mode of operation does not appear to have been put to practical use. Second, additional processing is required to obtain the spectrum from the raw interferogram - probably digital filtering and phase correction as well as the actual Fourier transform. With modern fast computers the processing of million-point interferograms is measured in seconds rather than minutes, but this requirement needs to be borne in mind when designing the system.

In summary, the SNR arguments favour an FT spectrometer against a scanning grating for most applications where either could be used. However, the high resolution and wavenumber accuracy achievable by FTS are not within reach of a grating spectrometer.

4 Fourier Transform Spectrometry in Practice in the VUV

There are two obvious reasons why FTS was not considered to be a suitable UV technique for many years after it was firmly established in the infrared. First, as has been shown above, the enormous gains in SNR offered by the multiplex and throughput advantages when the noise is independent of the signal (i.e., when it is detector-limited) are either non-existent or relatively small in the UV. Second, the construction of a scanning Michelson interferometer is perceived to be much more difficult in the UV because all optical and mechanical tolerances scale with wavelength, and the step from the near infrared to 200 nm is an order of magnitude. In this section we shall discuss design considerations and practical use of a relatively conventional scanning Michelson interferometer. The next two sections will deal respectively with non-scanning and all-reflection interferometers that avoid some of the limitations of VUV operation, at the expense of introducing other constraints. The final section describes a division-of-wavefront interferometer for the grazing incidence region.

In all cases the instruments described are state-of-the-art, and most of them are one-off

laboratory interferometers. This is in marked contrast to the situation in the infrared; FT-IR is a well-established market in which many manufacturers compete. Of these, only Bomem and Bruker [20, 21] have modified instruments with suitable beamsplitters to take them through the visible into the UV, and the Bruker specifies 220 nm as the end of its range. The Bomem DA8 claims a short wavelength limit of 180 nm, but, as shown below, the performance of any interferometer at wavelengths appreciably shorter than those for which it was designed degrades very rapidly. Similarly, the large laboratory IR/visible instruments built at Kitt Peak National Observatory [22] and Los Alamos [23] (the latter now being rebuilt at NIST) can justifiably claim to be UV spectrometers, but the effective limit of even the well-tried and high quality KPNO instrument is about 220 nm. The only scanning FT spectrometer designed specifically for the UV and actually working into the VUV is that built at Imperial College [24], a commercial version of which has been made by Chelsea Instruments [25].

4.1 The Michelson interferometer: technical considerations

The signal from the recombining wavefronts in a Michelson interferometer for a single frequency σ_o has so far been assumed to have the form of section 6.3, $I = I_o(1 + \cos 2\pi\sigma_o x)$, but this is true only for perfectly flat and parallel wavefronts. In practice the signal is

$$I = I_o(1 + m\cos 2\pi\sigma_o x) \tag{23}$$

where the modulation m, sometimes called the visibility, is given by

$$m = \frac{I_{max} - I_{min}}{I_{max} + I_{min}} \tag{24}$$

for intensities measured at zero path difference. The modulation is governed by the deviations from uniform phase over the whole area of the wavefront that is used. A local deviation ϵ in optical path difference causes a phase deviation of $2\pi\epsilon/\lambda$, and the rule of thumb for acceptable modulation is $\epsilon < \lambda/4$. For example, two perfectly flat wavefronts inclined at an angle such that the extreme path differences are $\pm\lambda/4$ give approximately 70% modulation (the exact value depends on whether the wavefront area is circular or rectangular). If the wavefronts are parallel but have random deviations from flatness, the modulation is 73% when the rms deviation is $\lambda/8$. As each of the recombining wavefronts has undergone at least one transmission and two reflections, the tolerance for each of the transmitting or reflecting optics should be set at $\lambda/8$ or better for the shortest wavelength of interest.

The penalty for low modulation is poor SNR. Whereas the entire dc signal contributes to the noise, it is only the modulated fraction that contributes to the signal. Thus the SNR is directly proportional to m. For a given value of ϵ_{rms} the modulation falls off exponentially with $(\epsilon_{rms}/\lambda)^2$, and the behaviour for other types of wavefront error is similar. For a given interferometer there will be some wavelength above which the modulation has an acceptable value, say 50%; below this wavelength m falls rapidly while the noise in the transformed spectrum, as we have seen, remains approximately constant. The SNR in the spectrum therefore drops, and the interferometer may have an effective short-wavelength cut-off that is well above the transmission limit of the optics.

Figure 6.6 shows schematically a conventional Michelson interferometer with plane mirrors, one of which is moved to record the interferogram. Evidently the collimating and focusing lenses can be replaced with mirrors, so that the only transmitting elements are the beamsplitter and compensating plate. For the UV these are made of fused silica, which can be used into the VUV down to about 180–170 nm, depending on the quality and thickness of the material. This material can be polished very flat and is also very homogeneous. This last point is important, because each of the separated beams is transmsitted through one of the plates – twice in the

arrangement of Fig. 6.6 and once in that of Fig. 6.7. For a 20 nm error ($\lambda/8$ at 160 nm) and a plate thickness of about 6 mm used at 45° the refractive index must be uniform to almost one part in 10^6. Below the transmission limit of fused silica it is necessary to use a crystal as beamsplitter. Very pure crystal quartz can transmit to ~160 nm, but its homogeneity is in doubt. Of the other VUV-transmitting crystals, CaF_2 extends to about 130 nm, MgF_2 to about 120 nm, and LiF almost to 100 nm, depending of course on the thicknesses used. As LiF is very difficult to polish, the material of choice is MgF_2. Although this can be polished adequately, the question of adequate homogeneity is less easy to answer; VUV refractometers do not exist, and measurements at longer wavelengths are of doubtful validity because of the non-linear behaviour of refractive index with wavelength.

The other critical tolerances are those for the surface quality and parallelism of the two mirrors, for the quality (guidance and smoothness) of the drive throughout a scan of several centimetres, and for maintaining the parallelism of the mirrors through this scan. Taking the last point first, the allowed tilt angle for the $\lambda/4$ extreme path difference specified above and for a beam diameter of 25 mm is 25 microradians, or 5 arcsec, at 120 nm. This cannot be achieved without active adjustment during the scan. The Bomem spectrometer referred to above uses the sampling He-Ne laser to monitor the parallelism and adjust the fixed mirror to compensate for tilt errors in the moving mirror. The alternative is to replace the fixed mirrors with tilt-invariant retroreflectors, which is the approach adopted in the Bruker, KPNO, Los Alamos, Imperial College and Chelsea Instruments interferometers. The Bruker has cube-corner retroreflectors, and all the others use catseyes, having a parabolic primary mirror and a small secondary mirror located accurately at its focus. Although the retroreflector ensures that the wavefronts remain accurately parallel, it does introduce an additional tolerance to be met, that of shear, which arises if the catseye does not move accurately along the optic axis of the interferometer. The shear tolerance is governed by the field of view, which in turn is limited by the resolving power required (equation 6.2); for high resolution at 120 nm it is of order 10 μm over the length of the scan. Tilting a retroreflector introduces shear as a second-order effect, but the resulting tilt tolerance is an order of magnitude less stringent than it is for a plane mirror. An incidental advantage of retroreflectors is the ability to offset the return beam from the incident beam and thus gain access to the complementary interferogram travelling back towards the source from the beamsplitter. Figure 6.7 shows schematically the layout of the Imperial College/Chelsea Instruments UV FT spectrometers [24] in which both outputs are used.

In most of the instruments mentioned above the guidance and drive requirements are met by using oil bearings and linear motors. The IC/CI interferometers have successfully exploited a simple rolling bearing in which the moving catseye is carried on three 14 mm balls, two of which are constrained by an accurately machined vee-block rail. One instrument uses a linear motor drive and the other a hydraulic drive; both of these have performed successfully.

The final tolerance to be considered is that of sampling the interferogram. The sampling interval Δx is determined by the free spectral range required (equation 6.17). As already stated, in practice the sampling intervals are derived from the interference fringes of a He-Ne laser (633 nm, corresponding to a wavenumber of 15798 cm^{-1}) following a path through the interferometer similar to that of the signal beam. In the infrared the samples can be taken at intervals of a whole fringe, or even several fringes, but the free spectral range of about 8000 cm^{-1} obtained from one sample per fringe is only about 20 nm in the VUV. It is therefore almost always necessary to subdivide the laser fringes to some degree: 10 samples per fringe would be required to satisfy the sampling theorem through the region down to 120 nm defined by a MgF_2 beamsplitter, but, as discussed in section 6.3.2, it is common practice to undersample. A fringe division of 3.5, for example, allows the region 180-120 nm to be recorded in the third alias, as illustrated in Fig. 5b,c. Periodic errors in the sampling interval give rise to ghosts, while random errors produce noise; in both cases the effect is approximately proportional to the fractional error in the sampling step

[17], so SNRs of a few hundred demand sampling accuracy of about one thousandth of a laser fringe. The interferometers referred to above achieve this sort of accuracy, using in some cases commercial systems adapted for the purpose. However it is difficult to eliminate entirely 'laser ghosts' arising from small systematic errors in the sub-division that repeat with the period of the laser fringes.

In practice when working in the VUV the bandwidth of the detected radiation is limited as far as possible, partly to allow undersampling but more importantly to avoid the noise that is spread all through the spectrum from radiation outside the spectral region of interest. Unfortunately VUV interference filters are expensive and not very efficient, and short-pass filters that exclude the near-UV but pass the VUV do not exist. The alternative is to use a detector with a long wavelength cut-off: the conventional solar-blind Cs-Te photocathode is insensitive above about 320 nm, and a more drastic cut-off at about 180 nm is possible by using Cs-I – well matched to the example of undersampling given above. For absorption experiments conducted with synchrotron continuum radiation the 'filter' problem is solved, in principle, by the provision of a monochromator as part of the standard equipment, but the effects of the dispersion need to be considered, as discussed at the end of section 6.4.2. It must be remembered when using a high alias that even if a suitable optical filter is in place there will still be additional noise folded in unless a matching electrical bandpass filter is used, either analogue or digital. Provided this precaution is taken, the SNR is independent of the free spectral range for the same total integration time.

4.2 Applications of VUV FTS

Emission spectrometry in the VUV has been mainly concentrated on the improvement of the database for the interpretation of astrophysical observations from space-borne instruments. This spectral region is rich in lines of the first ionisation stage of the transition element spectra, and accurate wavelengths and intensities are required both for reliable linelists and for the spectral analysis that is required to classify the large number of unidentified lines. In some cases the high resolution yields hyperfine structure and isotope splitting information. The usual light source for this work is a hollow cathode discharge, run at currents up to an ampere or so. Figure 6.8 shows part (about 15 nm) of the VUV spectrum from a 20 mA platinum-neon hollow cathode lamp at a resolving power of about one million, with a small section expanded to show the resolved line profiles, the assymetry of which is due to hyperfine structure. The integration time for the spectrum covering 180-140 nm was about 30 minutes, and the normalisation is for unit rms noise, so the ordinates represent the SNR.

The main limitation of FTS for this work is the fall-off of efficiency towards short wavelengths, primarily due to the decreasing modulation [26]. Although the transmission of a MgF_2 beamsplitter is still adequate at 120 nm, in practice it has proved difficult to avoid losing the signal in the noise before this limit is reached. The two other disadvantages that FTS has against a multi-channel grating spectrometer (using either a photographic plate or an array detector) are: (i) the SNR is worse for very weak lines (see section 6.3.4), and (ii) the SNR is also likely to be worse for the pulsed sources that may be needed to excite high stages of ionisation because of the effects of shot-to-shot irreproducibility. The two techniques should be regarded as complementary in the VUV, with FTS providing the high quality information for the stronger lines within its wavelength range and grating spectrometry extending the range for wavelength, intensity and excitation.

Absorption spectrometry in the VUV suffers from the lack of a bright and stable laboratory source of continuum radiation. The high pressure Xe arc falls rapidly in intensity below 200 nm, and deuterium lamps, while stable, are not very bright and are dominated by band structure below 160 nm. High current positive column hydrogen discharges are brighter than the commer-

cial deuterium lamps, but tend to be less stable and suffer the same breakdown into molecular band structure. The argon mini-arc is the only other laboratory source that can be used into the VUV. The alternative is synchrotron radiation, and this has indeed been successfully tried [26].

The less favourable spectral filling factors from a quasi-continuous source (see section 6.3.4 again) result in long integration times for good SNR, even with the high photon flux from a synchrotron. It is strongly advisable whenever possible to limit the bandwidth to the spectral region of interest, thus introducing an effective 'filling factor'; the SNR is then proportional to the inverse square root of the bandwidth. A premonochromator has obvious advantages over an interference filter because the centre and width of the band can be exactly matched to the requirements and the band edges are more sharply defined. Ideally this should be a double monochromator with zero net dispersion so that all wavelengths in the bandpass enter the interferometer at the same angle. With a standard single monochromator it is necessary to correct for the phase and wavelength shifts across the bandpass. It should be noted that there is no net gain in dividing a wide spectral band into several sections by selecting a narrow bandwidth for the monochromator because the gain in SNR for each individual section is cancelled by the necessity for recording several sections.

5 Spatially heterodyned, non-scanning interferometers for FTS

Non-scanning interferometers employ some form of multi-channel detector to record all elements of an interferogram simultaneously, rather than recording them sequentially with a single detector. They offer obvious advantages of ruggedness and stability, together with disadvantages in respect of flexibility and free spectral range. In the form first proposed, the technique was known as holographic FTS; it was achieved by slightly tilting one of the mirrors of a conventional Michelson interferometer, thus producing wedge fringes localised in the plane of the mirrors. These fringes were imaged onto a photographic plate [27]. For a small wedge angle α between the recombining wavefronts, the optical path difference is $x \sin \alpha$ where x is the distance along the plate from zero path difference. The interferogram is thus given by equation 6.13 with x replaced by $x \sin \alpha$, and it can be Fourier transformed in the normal way.

Modern versions of this interferometer replace the photographic plate with an array detector. This immediately focuses attention on the conflicting requirements of free spectral range and resolution. From equation 6.18 we see that the number of independent points N is the same in both the spectrum and the interferogram, and evidently N is now limited by the number of pixels in the detector. Thus for 1024 pixels the maximum resolving power would be only one thousand, or, taking proper sampling into account, 500. The breakthrough to a useful resolving power came with the introduction of a spatial heterodyning technique [28]. The mirrors are replaced by a pair of diffraction gratings set at the Littrow angle θ for a particular wavenumber σ_o at one end of the desired bandpass, as shown in Fig. 6.9. For this wavenumber the recombining wavefronts are parallel, and the spatial frequency of the interference fringes is zero. The gratings are oppositely tilted, so that for adjacent wavenumbers σ, either larger or smaller than σ_o, the wavefronts are inclined at some angle 2α that depends on $\mid \sigma_o - \sigma \mid$ and the angular dispersion of the gratings. For small values of α the grating equation gives for the spatial frequency f_x of the fringes along the x-axis

$$f_x = 4 \mid \sigma_o - \sigma \mid \tan \theta$$

The equation equivalent to 6.13 is then

$$I(x) = \int_0^\infty B(\sigma) \cos\{2\pi(4 \mid \sigma_o - \sigma \mid x \tan \theta)\} \, d\sigma \qquad (25)$$

Comparing this with equation 6.13, σ is replaced with $\sigma' \equiv \mid \sigma_o - \sigma \mid$ and x with $x' \equiv 4x \tan\theta$. The spectrum $B(\sigma')$ recovered from Fourier-transforming this interferogram therefore starts from σ_o instead of zero wavenumber.

The similarity of equations 6.13 and 6.25 makes it clear that the instrument function is a sinc function, as in equation 6.15, with L replaced by the maximum value X' of x'. If the interferometer is arranged to give zero path difference in the middle of the interferogram, the maximum value of x is half the projected width of the grating, $W\cos\theta/2$, giving $X' = 2W\sin\theta$. The resolution limit (cf. equation 6.16) is therefore

$$\delta\sigma = 1/2X' = 1/(4W\sin\theta) \tag{26}$$

which is just twice the diffraction-limited resolution of the individual gratings. Given that the number of independent spectral points is limited to the number N of detector pixels, the free spectral range is given by (cf. equation 6.18)

$$\Delta\sigma \equiv \mid \sigma_o - \sigma_m \mid = N\delta\sigma = N/(4W\sin\theta) \tag{27}$$

where σ_m is the maximum (or minimum) allowed wavenumber. The same result can be derived from the fringe spatial frequency f_x by setting its maximum value, $4 \mid \sigma_o - \sigma_m \mid \tan\theta$ equal to the sampling spatial frequency $N/(W\cos\theta)$ imposed by the detector. For further details see, e.g., [29, 30, 31] and references in these papers.

Some arrangements use only one grating, retaining a mirror in the other arm of the interferometer [29]; this leads to some loss of coherence and to drops of factors of two in the relations given above, but the overall picture is not affected. It is also possible to use two gratings of different spacing, tilted in either the same or opposite directions, to decrease or increase the path difference.

Spatially heterodyned FTS, or SHS, has exactly the same noise characteristics as scanning FTS. Provided the imaging of the fringes is correctly done, the throughput is limited by the resolving power in the same way. If the noise is photon-limited, the SNR is theoretically the same in the two techniques because the spread of the signal over N detectors is exactly compensated by the factor N in integration time per point gained from not scanning. For the source-noise limited case there is actually a gain of $\sqrt{N}$ in SNR.

The advantage or otherwise of SHS over a straightforward dispersion arrangement using the same grating (and hence the same resolving power) and the same detector also needs to be considered. As pointed out in section 6.3.4, FTS loses a factor of $\sqrt{N}$ in SNR to grating spectrometry when the latter has a multi-channel detector. This is counteracted by the throughput advantage of SHS – particularly if this can be increased by field-widening as described below. The SNR balance between the two techniques is normally in favour of SHS, but it should be assessed for any particular problem.It should also be noted that the use of a dispersive system compromises the high wavelength accuracy of scanning FTS [32].

It is important to remember the band-limiting constraints of SHS. The spectrum is effectively folded over at σ_o, with $\sigma_o + \Delta\sigma$ indistinguishable from $\sigma_o - \Delta\sigma$. Similarly, wavenumbers outside the range $\mid \sigma_o - \sigma_m \mid$ are aliased in the same way as in a scanning FT spectrometer that is undersampled. It is possible to get around the ambiguity problem by rotating one of the gratings through a small angle β about an axis in its plane, so that the grooves of the two gratings are no longer parallel. This produces an unheterodyned low resolution interferogram along the y-axis, in which $\sigma_o \pm \Delta\sigma$ are no longer degenerate, thereby doubling the free spectral range. By an extension of this idea, the gratings can be used in higher orders to produce a two-dimensional interferogram that can be transformed to yield a spectrum in an echelle-like format, with the overlapping orders of the high resolution spectrum along the x-axis separated by low resolution cross-dispersion along the y-axis [30].

The SHS technique has been mainly developed in two centres. The Astronomy group at Groningen have been primarily concerned with using it on large ground-based telescopes [29]. Of more relevance to the VUV region is the work of Roesler and his colleagues at Wisconsin [30, 31], who have developed the technique with a view to using it for space-based observations of diffuse interstellar emission lines. In its original form their interferometer still uses a transmitting beamsplitter; the all-reflection version is discussed in the following section. Elimination of the need to provide an accurate scanning mechanism is not only an advantage in itself, particularly of course for an instrument designed for space-flight applications, but also makes field-widening relatively simple: the addition of two thin prisms to the interferometer in fixed positions, one in front of each of the gratings, increases the throughput by two orders of magnitude [30, 31].

As pointed out by Harlander *et al.*[31], an additional and more subtle advantage of the SHS in the VUV is the relaxation of tolerances in the figure of the various surfaces and the homogeneity of the beamsplitter. This comes about because the interference fringes are localised in the plane of the gratings, so the grating surfaces are imaged on the detector. Each pixel therefore sees only a small element of the grating area. Similarly, the beamsplitter is closely enough in focus that only a relatively small part of its area contributes to each pixel. Wavefront errors on a scale larger than the pixel area affect the fringe shape or spacing, but they do not degrade the fringe contrast as they do when the entire wavefront is imaged onto a single detector. Any errors in fringe shape can be detected directly and corrected for in software. In view of the uncertainties about optical homogeneity near the transmission limits of the crystals, this is potentially a very important advantage.

6 All-reflection FT spectrometers

For wavelengths shorter than about 120 nm, FTS is possible only with an all-reflection interferometer. Even for rather longer wavelengths there are potential advantages in getting away from the stringent requirements placed on the crystal that is used as beamsplitter. An all-reflection interferometer with a division-of-wavefront beamsplitter, using grids or apertures, is relatively simple to design (in principle, anyway), but considerable effort has gone into a division-of-amplitude reflecting system in order to maintain the throughput advantage.

The concept of a reflection diffraction grating as a division-of-amplitude beamsplitter was suggested as early as 1959 – see references given in the paper by Kruger *et al.*[33], who proposed a practical form of scanning interferometer and tested it in the UV, although not in the VUV. The wavelength dispersion is an inevitable, but undesirable, property of the grating when it is used as a beamsplitter; in order to maintain coherence of the recombining wavefronts over a wavelength range wider than the resolution of the grating, it is necessary to cancel the dispersion. Kruger *et al.*[33] did this with an additional pair of gratings, one in each arm of the interferometer. In one of their designs these gratings were additional to the plane mirrors, one of which was scanned [34]; in another design the plane mirrors were eliminated to reduce the number of reflections, and one of the gratings was scanned [33]. This second design introduced a wavelength-dependent path difference, which distorted the wavelength scale in the transformed spectrum and had to be corrected for.

The availability of UV-sensitive array detectors and the development of the SHS technique combined to make feasible an all-reflection non-scanning interferometer, in which the dispersion of the grating is actually used to produce the required path difference. Recent work on all-reflection normal incidence FT spectrometers appears to have been confined to developing different configurations for SHS. The simplest version, as proposed by the Wisconsin group [30, 32], is shown in Fig. 6.10. The grating acts as beamsplitter and at the same time introduces a wavelength-dependent wedge angle between the recombining wavefronts. Zero spatial frequency for the interference fringes corresponds to the wavenumber σ_o for which the diffracted

rays are normal to the mirrors, and the interferogram has exactly the same characteristics as that produced by the transmitting beamsplitter system described in the last section. In plan the output beam returns along the same path as the input beam, but it is shifted out of plane by a slight tilt, so that the two beams use respectively the upper and lower halves of the aperture.

Figure 6.11 shows another design developed for the EUV region [32, 35], using a common path configuration in which one half of the grating acts as beamsplitter and the other half as beam recombiner. The divided beams travel round the system parallel to one another but in opposite directions. This design is particularly robust because any small disturbances to the components affect both beams equally, at any rate to first order. This design has been tested at Lyman α with a grating of 600 lines/mm in the second order and found to achieve 80% of its theoretical resolution [35], which is set by the half-width of the grating that is illuminated by the incident beam. To emphasize the bandwidth restrictions, it should be noted that at the resolving power of 120000 offered by the grating the free spectral range allowed by a detector of 512 pixels is only about 0.25 nm.

As with the transmission SHS described in the last section, it is possible to double the free spectral range by introducing a small tilt of the mirrors to produce an unheterodyned interferogram in the y-direction. In the same way it is also possible to exploit higher orders to give an echelle-like format [32]. The principal difference in the characteristics of the all-reflection and the transmission versions of SHS is the loss of a factor $\cos\theta$ in the throughput of the former, arising from the fact that the grating is not used in the Littrow configuration. The number of reflections in the two versions is similar, but the optical efficiency in the reflection interferometer is reduced by the need for the grating blaze to throw equal energy into the orders either side of the normal.

7 Soft x-ray FTS by grazing reflection

In order to progress below about 40 nm it is necessary to adopt a grazing-incidence reflection geometry and this is being attempted by a group at the Advanced Light Source synchrotron-radiation facility in Berkeley, USA [36]. The construction of an interferometer in this spectral region poses significant new mechanical challenges which we describe below. The required technical solutions provide an indication of the type of effort involved in extending FTS to cover the entire VUV region. The present motivation is to achieve higher resolution than a grating for studies of two-electron excitations in helium near the double ionization region (60-80 eV). The original discovery, in 1963, of autoionizing series in the absorption spectrum of helium [37] was an early triumph of synchrotron-radiation spectroscopy, achieved at Gaithersberg. Subsequent work at Berlin [38, 39] (at 4 meV resolution) and later at Berkeley [40] (at 1 meV) has revealed further series, and these measurements (all by grating spectrometers) continue to excite strong interest in the theoretical-atomic-physics community.

At grazing incidence it is essentially impossible to use the same beam splitter for both division and recombination of the wave fronts, so the traditional Michelson geometry and its variants have to be abandoned in favor of a Mach-Zehnder type of layout [1, 41]. In the Berkeley scheme the normal rectangular shape of the latter has been deformed into a rhombus, and extra mirrors have been added to allow the path difference to be scanned (see Fig. 6.12). The system presently under test has a path difference of $\pm$ 17 mm which implies a potential resolving power of more than one million at 20 nm (see section 3.3).

The spectrometer to be described here will be fed by a beam of synchrotron radiation from a low-resolution monochromator on an Advanced-Light-Source bending-magnet beam line. The light from such a monochromator will have a fractional bandwidth ($1/W_{\rm in}$) of about 1/500 which is unusually narrow for an FTS source. This situation has some noteworthy features.

1. A grating spectrometer can often accept all of the light from a high-brightness synchrotron-radiation beam. In such a case, neither the throughput (Jacquinot) nor multiplex (Fellgett) advantages exist, and it is again the resolution advantage that is being sought via FTS (see section 6.1).

2. With a narrow-band input spectrum and a path-difference scanning rate v, the expected interferogram (see equation 6.15) is close to a pure cosine wave of temporal frequency $v\sigma_m$. This cosine signal acts as a carrier wave on to which the spectral information is modulated as an envelope function that varies slowly in both amplitude and phase. The centre (temporal) frequency of the incoming wave is down-shifted by a factor v/c (section 6.3.1) so that for an experiment at 20 nm, an output at 1 kHz can be produced with $v = 20$ μm/sec. A frequency in this range is suitable for working with synchrotron sources which tend to suffer from small beam motions (noise) at frequencies below about 100 Hz.

3. Since only one W_{in}th of the spatial frequency range from zero to σ_m will contain any signal, the interferogram can be under-sampled by a factor W_{in}, which is equivalent to sampling the envelope function at *its* Nyquist frequency. In the terms of section 6.3.2 this means the system will be working in the W_{in}th alias, and the same conditions indicated there must be satisfied.

The first requirement for a grazing incidence interferometer is a beam splitter, and at 20° grazing angle and 20 nm wavelength a transmission device is impractical. The closest one can get to an amplitude-division beam splitter is therefore a type of transmission grating used in zero order. Although such a device actually divides the *wavefront*, it may still produce a final result similar to amplitude division, provided it has a sufficiently small period and enough propagation distance is allowed for the dissected wavefronts to be smoothed by diffraction. Such a grating must be quite unusual, however, because the front faces of the opaque bars must form a planar reflecting surface of wave front-preserving accuracy. Several transmission-grating beam splitters of this type with 100μm period have now been constructed by photolithography and directional etching of silicon [42] (Fig. 6.13). The reflecting surfaces obtained were flat within 0.6 μradian rms and smooth within 2 Å rms.

The flexural mechanism [43] used to translate the table carrying the four mirrors (Fig. 6.12) by ±7.5 mm has been constructed by electric-discharge machining (spark erosion) of a monolithic block of type C300 maraging steel. It includes a moving table which carries a special prism on to which all four mirrors are optically contacted. The design is a classical double-sided compound rectilinear spring [44, 45], and to obtain such a large motion with reasonable stresses, the hinges are implemented as monolithic crossed strips [46, 47]. The mechanism, which is about the size of a notebook computer, can be seen with the table at one end of its travel in Fig. 6.14. The rms tilt error of the table in the pitch direction over the 15 mm motion has been measured to be 0.38 μradian, leading to a wave front tilt error of 0.57 μradian.

The possibility of realizing the theoretical resolution of soft x-ray FTS depends on being able to manufacture the spectrometer and optics within the required tolerances (see section 6.4.1). Some of the tolerances and achieved values for the Berkeley system are summarized in Table 1. The underlying goal is a relative tilt between the interfering wave fronts of less than 1.5 μradian, which should give greater than 90% of the maximum possible modulation.

The optics of Michelson and Mach-Zehnder interferometers are discussed in standard texts [1, 41, 48]. For a point source and a perfectly built system with no mirror tilts the situation is quite straightforward. Viewed from the detector there are, in general, two virtual point sources at different distances, and the observation space is filled with a single concentric ring pattern which is visible everywhere. Such a fringe system is said to be non-localized and a FTS experiment would proceed by placing a detector inside the center fringe of the system (see

Table 1: Mechanical and optical tolerances

Quantity	Required	Achieved
Table rms tilt errors	*(quadratic sum	0.57 μrad
Mirror1 rms slope errors	*(of all four	0.7 μrad
Mirror2 rms slope errors	*(rms tilts	0.7 μrad
Beamsplitter rms slope errors	*($< 1.5\mu$rad	0.6 μrad
Table motion rms indexing error	< 8 Å	4 Å (noise limit)
Driver rms stick-slip (diff.from linear motion)	< 8 Å	4 Å (over 1 sec)

section 1 by equation 6.2). On the other hand, if the source becomes extended, most of the pattern disappears and the fringes become localized, which means in this case that they can only be observed in the focal plane of a lens. Such "fringes of equal inclination" have already been discussed in section 6.1.

The blurring of the non localized fringe pattern by the increase of the source size can be understood as a degradation of the coherence of the optical field, and with this viewpoint one can calculate the degree of extension of the source that can be tolerated if non-localized fringes are to remain visible with a given contrast. Such calculations can be accomplished using the van Cittert-Zernike theorem [41], which provides a prescription for calculating the complex degree of coherence $\mu(P_1,P_2)$ between two points P_1 and P_2 (μ is defined, for example, by Born and Wolf [41]). According to the theorem $\mu(P_1,P_2)$ is proportional to the amplitude that would be found at P_2 if a spherical wave converging toward P_1 were to be diffracted by an aperture function with the position and shape of the source intensity distribution. What is not always stated is that P_1 and P_2 need not be in the same plane, so that the theorem indicates the existence of a good-coherence volume determined by the wavelength and a 'numerical aperture' equal to the half angle subtended by the source – i.e., the angle θ of section 6.1. For a uniform circular source, the distance from the centre to the first zero of $\mu(P_1,P_2)$ is thus $0.61\lambda/\theta$ in the width direction and $2\lambda/\theta^2$ in the depth direction [49], similarly to a conventional resolution function.

Both the width and the depth of $\mu(P_1,P_2)$ are important for interferometry because the detection point P, viewed now from the source via the two interfering beams, appears as two points (P_1 and P_2). These points in general have both a longitudinal separation due to the intentional path difference of the instrument and a transverse separation due to mirror tilts. For the soft x-ray interferometer discussed here the numerical aperture is defined by the size and distance of the monochromator exit slit to be about 30 μradian. At $\lambda = 20$ nm this determines a depth resolution of many meters, which comfortably allows the required 17 mm path difference. It also defines a transverse coherence width at the interferometer of about a millimeter. The operational requirements are therefore that the period of the grating and any transverse separation of P_1 and P_2 (wave-front shears) that could be produced by mirror angle errors must be much less than 1 mm, both of which are easily achieved.

The conclusion from these arguments is that the soft x-ray interferometer will produce a single set of Haidinger fringes. This ring pattern will be nonlocalized and will fill the observation space, so that experiments should be possible without a 'lens' in the detection region. Such a clean interference pattern results to a large extent from the fact that the incoming beam of synchrotron light has a high degree of spatial coherence. For other situations in which short-wavelength FTS might be interesting, such as soft x-ray emission spectroscopy, the coherence of the source is usually much worse and the experiment correspondingly more difficult.

The detection system may be one of two types: a photo diode downstream of the helium cell that would register the transmitted signal or an ion chamber of which the working gas would be the helium sample. The first would provide a transmission spectrum, governed by equation 6.21, while the second would provide a signal analogous to that of an emission spectrum and would

be governed by equation 6.22. In either case the technical goal would be shot-noise-limited detection, which has been shown to be possible [50] at least in the case of a source with somewhat similar time structure to the sub-nanosecond pulses one gets from a synchrotron.

The ultimate uncertainty for applications of FTS to gas-phase soft-x-ray synchrotron-radiation experiments is whether the attainable modulation and photon rate will allow an experiment in a reasonable time. This has been addressed by the Berkeley group by means of computer modeling of the Rydberg series that converges to the lowest excited state of He^+ as parameterised by Domke *et al.*[39]. The average modulation of the interferogram (the standard deviation of the recorded intensity divided by its mean), calculated by Fourier transforming the known spectrum, was found to be 0.005 [36]. This, combined with realistic estimates of the number of photons arriving in the assumed collection time of 10^3 sec, leads, via equation 6.21, to a SNR in the final spectrum of 330. Although this value was calculated without allowance for experimental error, it did use the conservative assumption of a transmission experiment.

This calculation provides a conclusion to this section on soft-x-ray FTS experiments. We have shown that if a reasonable fraction of the maximum possible modulation can be achieved (and the mechanical requirements for that have mostly been met as described above), then the system will yield good spectra, and we therefore look forward to a successful experimental programme.

References

[1] W.H.Steel *Interferometry*, 2nd ed., Cambridge University Press, 1983

[2] P.Bousquet *Spectroscopy and its Instrumentation* (tr.K.M.Greenland), Adam Hilger, London, 1971

[3] G.Hernandez *Fabry-Perot Interferometers*, Cambridge University Press, 1986

[4] Y.Guern, A.Bideau-Méhu, R.Abjean and A.Johannin-Gilles, Opt.Commun. 12, 66-70, 1974

[5] A.Bideau-Méhu, Y.Guern, R.Abjean and A.Johannin-Gilles, J.Phys.E 13, 1159-1162, 1980

[6] A.Bideau-Méhu, Y.Guern and R.Abjean, J.Phys.E 17, 265-267, 1984

[7] T.Barbee and J.H.Underwood, Optics Comm. 48, 161-166, 1983

[8] R.J.Bartlett, W.J.Trela, D.R.Kania, M.P.Hockaday, T.W.Barbee and P.Lee, Optics Comm. 55, 229-235, 1985

[9] M.P.Bruijn, J.Verhoeven and M.J.Van der Wiel, Optical Engineering 26, 679-684, 1987

[10] L.Mertz *Transformations in Optics*, Wiley, New York, 1965

[11] R.N.Bracewell *The Fourier Transform and its Applications*, McGraw-Hill, New York, 1965

[12] J.Chamberlain, *The Principles of Interferometric Spectroscopy*, John Wiley, 1979

[13] P.R.Griffiths and J.A.de Haseth *Fourier Transform Infrared Spectrometry*, John Wiley, 1986

[14] G.A.Vanasse and H.Sakai in *Progress in Optics* (ed.E.Wolf), Vol.VI, 259-330, North-Holland, Amsterdam, 1967

[15] H.Sakai in *Spectrometric Techniques* (ed.G.A.Vanasse), Vol.I, 1-70, Academic Press, 1977

[16] G.Guelachvili in *Spectrometric Techniques* (ed.G.A.Vanasse), Vol.II, 1-62, 1980

[17] J.W.Brault, *Fourier Transform Spectrometry* in Proc.of 15th Advanced Course of the Swiss Society of Astronomy and Astrophysics (eds. a.O.Benz, M.C.E.Huber, M.Mayor), Saas Fee, 1985

[18] R.C.M.Learner, A.P.Thorne, I.Wynne-Jones, J.W.Brault and M.Abrams, J.Opt.Soc.Am. A12, 2165-2171, 1995

[19] J.W.Brault, Mikrochim.Acta 3, 215-225, 1987

[20] Bomem DA8, Hartman & Brown, Quebec, Canada

[21] Bruker IFS 120 HR, Bruker-Franzen Analytik Gmbh, Bremen, Germany

[22] J.W.Brault, Oss. Mem. Osservatorio Astrofisico di Arcetri 106, 33-50, 1978

[23] B.A.Palmer, Opt.Soc.Am. Technical Digest Series, Vol.6, 52-55, 1989

[24] A.P.Thorne, C.J.Harris, I.Wynne-Jones, R.C.M.Learner and G.Cox, J.Phys.E 20, 54-60, 1987

[25] Chelsea Instruments Ltd., East Molesey, Surrey KT8 0QX, UK

[26] A.Thorne, Physica Scripta T65, 31-35, 1996

[27] G.W.Stroke and A.T.Funkhouser, Phys.Lett. 16, 272-274, 1965

[28] T.Dohi and T.Suzuki, Appl.Opt. 10, 1137-1140, 1971

[29] S.Fransden, N.G.Douglas and H.R.Butcher, Astron.and Astrophys. 279, 310-321, 1993

[30] J.Harlander, R.J.Reynolds and F.L.Roesler, Astrophys.J. 396, 730-740, 1992

[31] J.Harlander, F.L.Roesler, R.J.Reynolds, K.Jaehnig and W.Sanders, *EUV, X Ray and Gamma Ray Instrumentation for Astronomy V* (ed.O.Siegmund), SPIE 2280, 1994

[32] J.Harlander and F.L.Roesler, *Instrumentation for Astronomy VII* (ed.D.L.Crawford), SPIE 1235, 622-633, 1990

[33] R.A.Kruger, L.W.Anderson and F.L.Roesler, Appl.Opt. 12, 533-540, 1973

[34] R.A.Kruger, L.W.Anderson and F.L.Roesler, J.Opt.Soc.Am. 62, 938-945, 1972

[35] S.Chakrabarti, D.M.Cotton, J.S.Vickers and B.C.Bush, Appl.Opt. 33, 2596-2607, 1994

[36] M.R.Howells, K.Frank, Z.Hussain, E.J.Mohler, T.Reich, D.Möller and D.A.Shirley, Nucl.Instrum.Meth. A 347, 182-191, 1994

[37] R.P.Madden and K.Codling, Phys.Rev.Lett. 10, 516-518, 1963

[38] M.Domke, C.Xue, A.Puschman, T.Mandel, E.Hudson, D.A.Shirley, G.Kaindl, C.H.Greene and H.R.Sadeghpour, Phys.Rev.Lett. 66, 1306-1309, 1991

[39] M.Domke, G.Remmers and G.Kaindl, Phys.Rev.Lett. 69, 1171-1174, 1992

[40] K.Schultz, G.Kaindl, M.Domke, J.D.Bozek, P.A.Heimann and A.S.Schlachter, Phys.Rev.Lett. 77, 3086-3089, 1996

[41] M.Born and E.Wolf, *Principles of Optics*, 6th Edition, Pergamon, Oxford, 1980

[42] Boeing North American, 2511C, Broadbent Avenue Parkway NE, Albuquerque, NM 87107, USA

[43] S.T.Smith and D.G.Chetwynd, *Foundations of Ultraprecision Mechanism Design* (1st Edition), Gordon and Breach, Reading, 1993

[44] M.R.Howells, Advanced Light Source Technical Report, LSBL 212, Lawrence Berkeley National Laboratory, 1994

[45] Smith & Chetwynd, *op. cit.*, Fig. 4.8

[46] M.R.Howells, R.Duarte and R.McGill, Advanced Light Source Technical Report, LSBL 213, Lawrence Berkeley National Laboratory, 1994

[47] Smith & Chetwynd, *op. cit.*, Fig. 4.16b

[48] J.Dyson,*Interferometry as a measuring tool*, Machinery Publishing Co., Brighton, 1970

[49] Born & Wolf, *op. cit.*, paragraph 8.8.2

[50] E.M.Gullikson, J.H.Underwood, P.C.Batson and V.Nikitin, J. X-Ray Sci.Technol. 3, 283-299, 1992

[51] Hewlett-Packard, Test and Measurement Division, Mail stop 51 LSJ, PO Box 58199, Santa Clara CA 95052-9952, USA

Figure Captions

1. The path difference x between the two beams reflected from parallel surfaces separated by t is given by $x = t \sec\theta(1 + \cos 2\theta) = 2t\cos\theta$, where θ is the angle of incidence..

2. Complex amplitudes of successive reflections in F-P interferometer. τ and ρ are the coefficients of transmission and reflection respectively, and ϕ is the phase increment, given by $\phi = 2\pi x/\lambda = 4\pi\sigma t\cos\theta$.

3. Airy distribution as a function of optical path difference x for two different reflectivities, R=0.7 and R=0.9.

4. The intensity distribution sinc$2\sigma L$ for a monochromatic line at σ_o. The first zeroes are at $\sigma - \sigma_o = \pm 1/2L$.

5. The effects of the interferogram sampling interval on the recovered spectrum. The spectrum and its mirror image are replicated at intervals of $1/\Delta x$, as shown in (a), where the Nyquist condition $\Delta x \leq 1/2\sigma_m$ is fulfilled. If the spectrum is limited to a finite band, $\sigma_1 \rightarrow \sigma_2$, it is possible to under-sample without ambiguity, as shown in (b), provided that $\Delta x\,(\equiv 1/2\Delta\sigma) \leq (\sigma_2 - \sigma_1)$. The spectrum is then 'aliased' into the empty lower frequency regions as if folded backwards and forwards, as illustrated in (c).

6. Conventional scanning Michelson interferometer. A = entrance aperture, B = beamsplitter, C = compensating plate, D = detector. M_1' is the image of M_1, distant t from the scanning mirror M_2.

7. Schematic diagram of scanning VUV FT spectrometer configuration (see ref.24). A = entrance aperture, B = beamsplitter/recombiner, C_1, C_2 = catseye retroreflectors, P_1, P_2 = photomultipliers detecting the two output signals. M_1, M_3 and M_4 are concave mirrors and M_2 is a folding plane mirror.

8. Part of the VUV spectrum of a 20 mA platinum-neon hollow cathode lamp taken with the Imperial College FT spectrometer in the spectral region 160-145 nm, using a MgF_2 beamsplitter. The resolution is 0.06 cm^{-1}, corresponding to a resolving power of about one million. The strong 'line' in the top plot is actually two lines separated by 0.015 nm, as shown in the expanded section, and the line asymmetry is due to unresolved hyperfine structure.

9. Schematic diagram of the basic SHS configuration, using a transmitting beamsplitter BS. Wavelength-dependent Fizeau fringes produced by diffraction gratings G_1 and G_2 are focused onto the imaging detector (see ref.32).

10. Schematic diagram of the basic all-reflection SHS configuration. Light enters the system through the upper half of split aperture S and exits through the lower half. The mirror M_4 focuses the fringes onto the imaging detector I. The diffraction grating G_o acts as both the beamsplitter and the dispersive element in the system (see refs.30, 32).

11. All-reflection common path SHS configuration. Light enters through the collimator C, and the grating G splits and recombines the two beams (dotted and dashed lines), which traverse the system in opposite directions. The converging mirror M_3 images the interference fringes onto the detector I (see refs.32, 35).

12. Layout of the grazing-incidence Mach-Zehnder interferometer for use at 20 nm wavelength. The normal rectangular layout has been deformed into the rhombus ABCD, and four mirrors, all mounted to the same table, are used to enable the path difference to be scanned. This is accomplished by translating the table in the direction of the arrows. In this figure the system is at zero path difference while in Fig. 6.14 it is shown at maximum path difference.

13. Geometry of the transmission grating beam splitter, made by optical polishing followed by photolithography and directional etching of silicon.

14. The flexure mechanism for scanning the optical path difference. The outer frame of the mechanism FF' carries the two beam splitters which are fixed in position. The four mirrors are fixed to the moving table TT' here shown driven to one extreme of its travel. One side of the table is (kinematically) connected to a drive shaft activated by a double-sided hydraulic piston while the other side carries a retroreflector by which its position is measured with a laser interferometer [51].

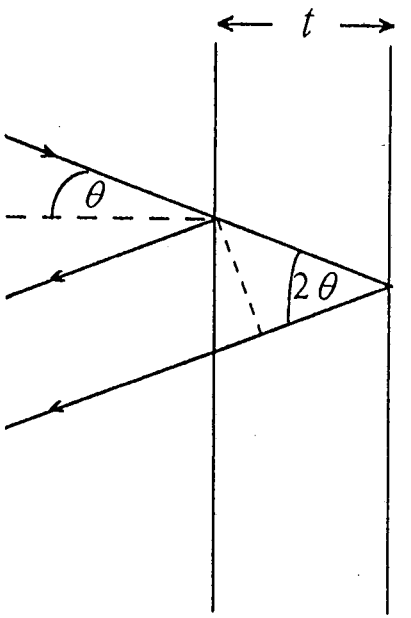

Figure 1

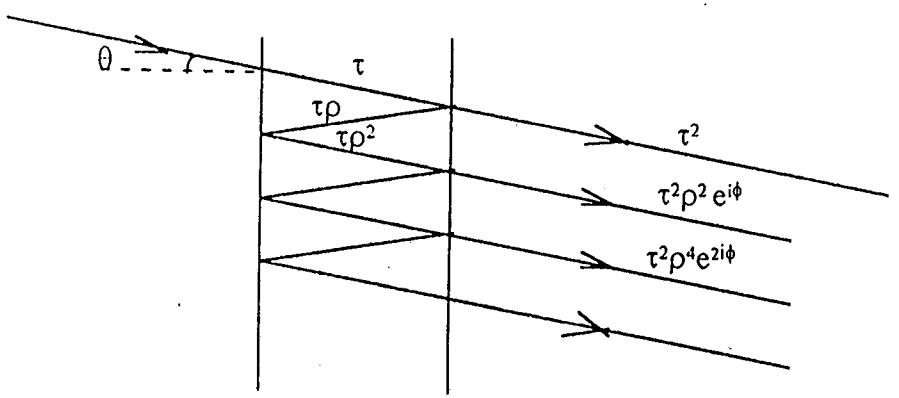

Figure 2

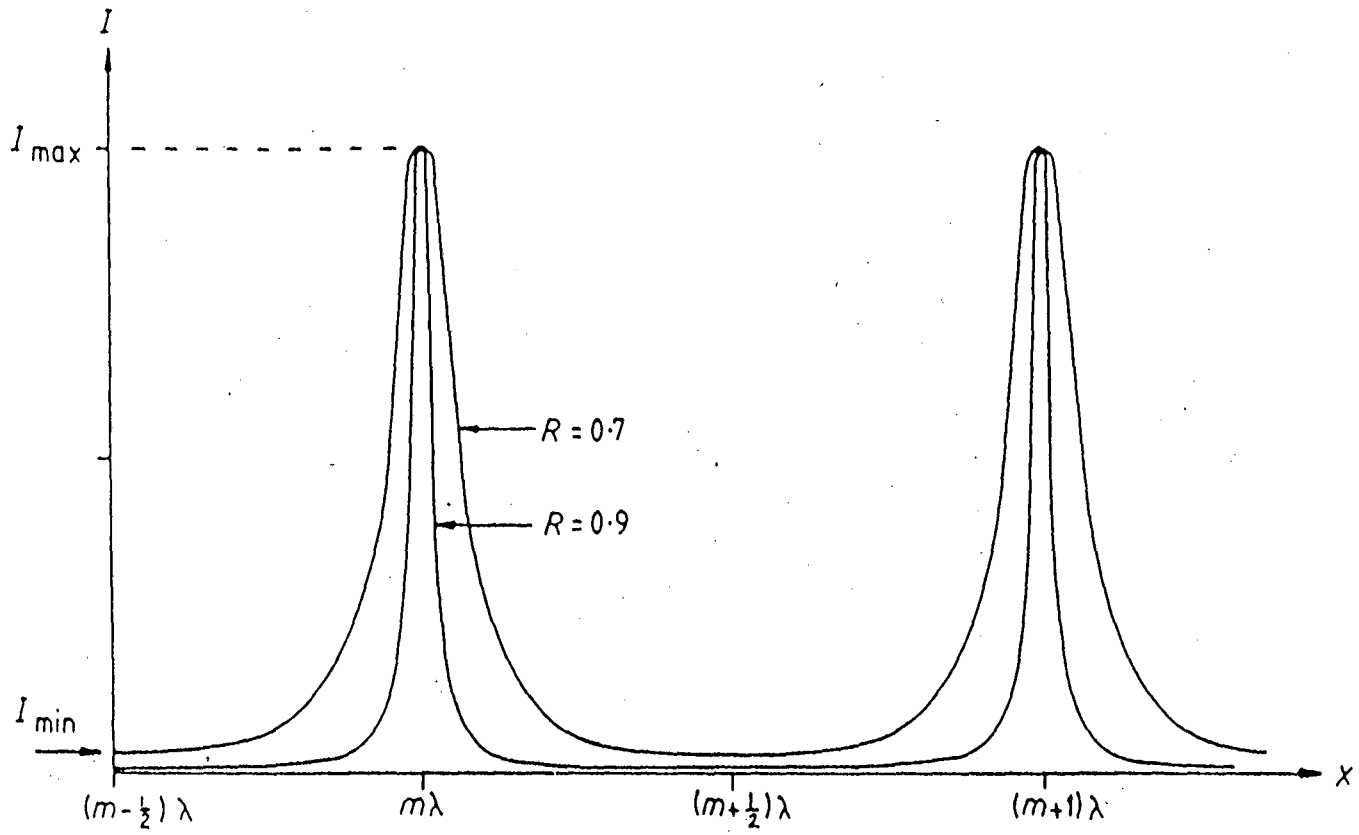

Figure 3

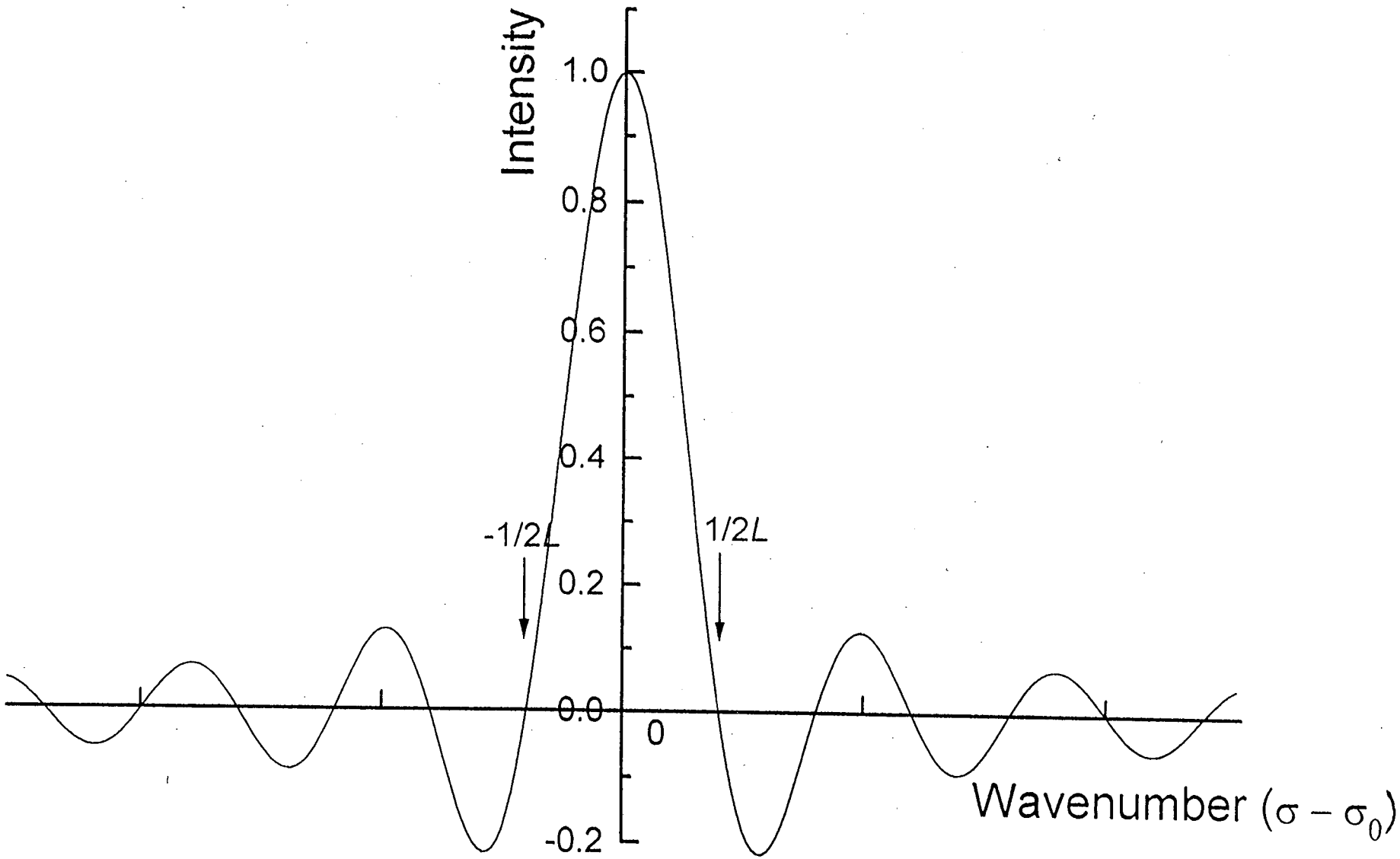
Intensity
1.0
0.8
0.6
0.4
0.2
0.0
-0.2
-1/2L
1/2L
0
Wavenumber ($\sigma - \sigma_0$)

Figure 4

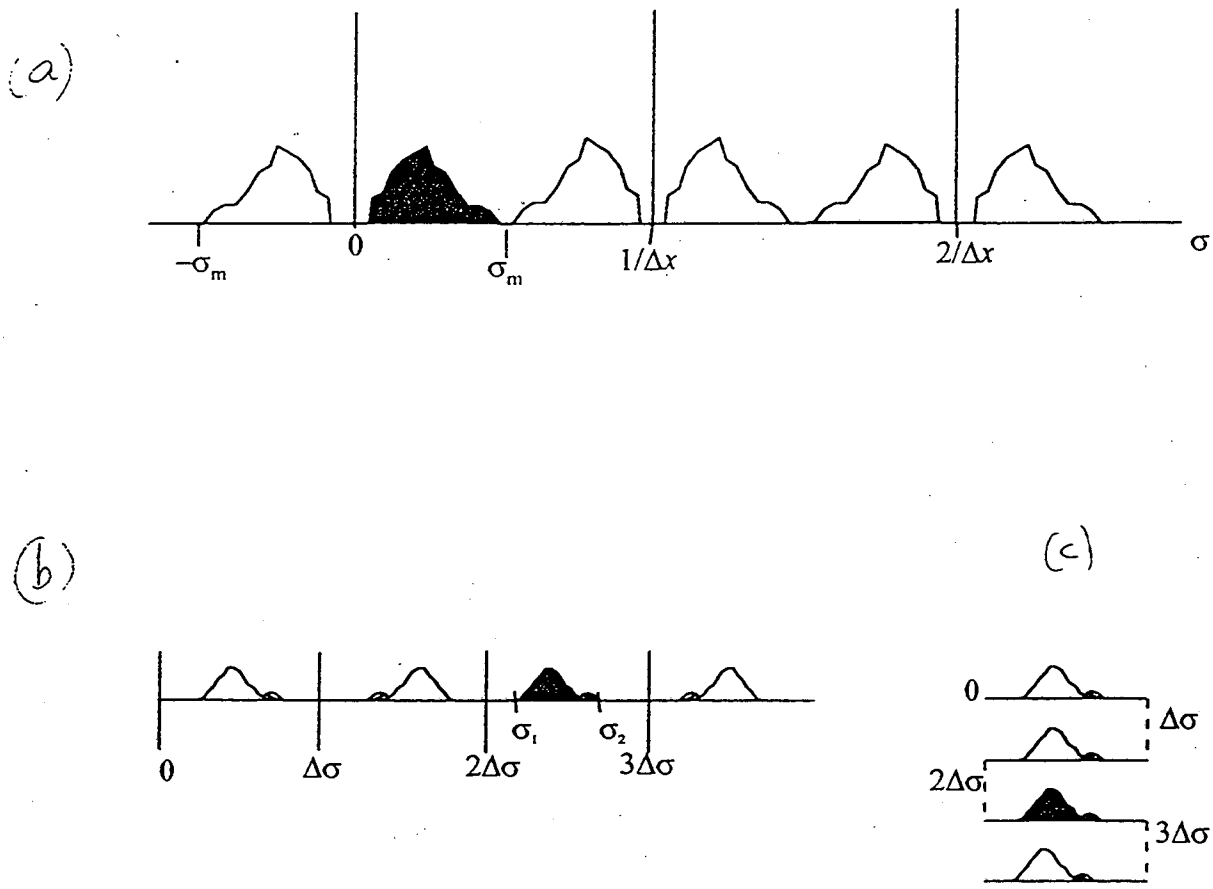
(a)
$-\sigma_m$
0
σ_m
$1/\Delta x$
$2/\Delta x$
σ
(b)
0
$\Delta\sigma$
$2\Delta\sigma$
σ_1
σ_2
$3\Delta\sigma$
(c)
0
$\Delta\sigma$
$2\Delta\sigma$
$3\Delta\sigma$

Figure 5

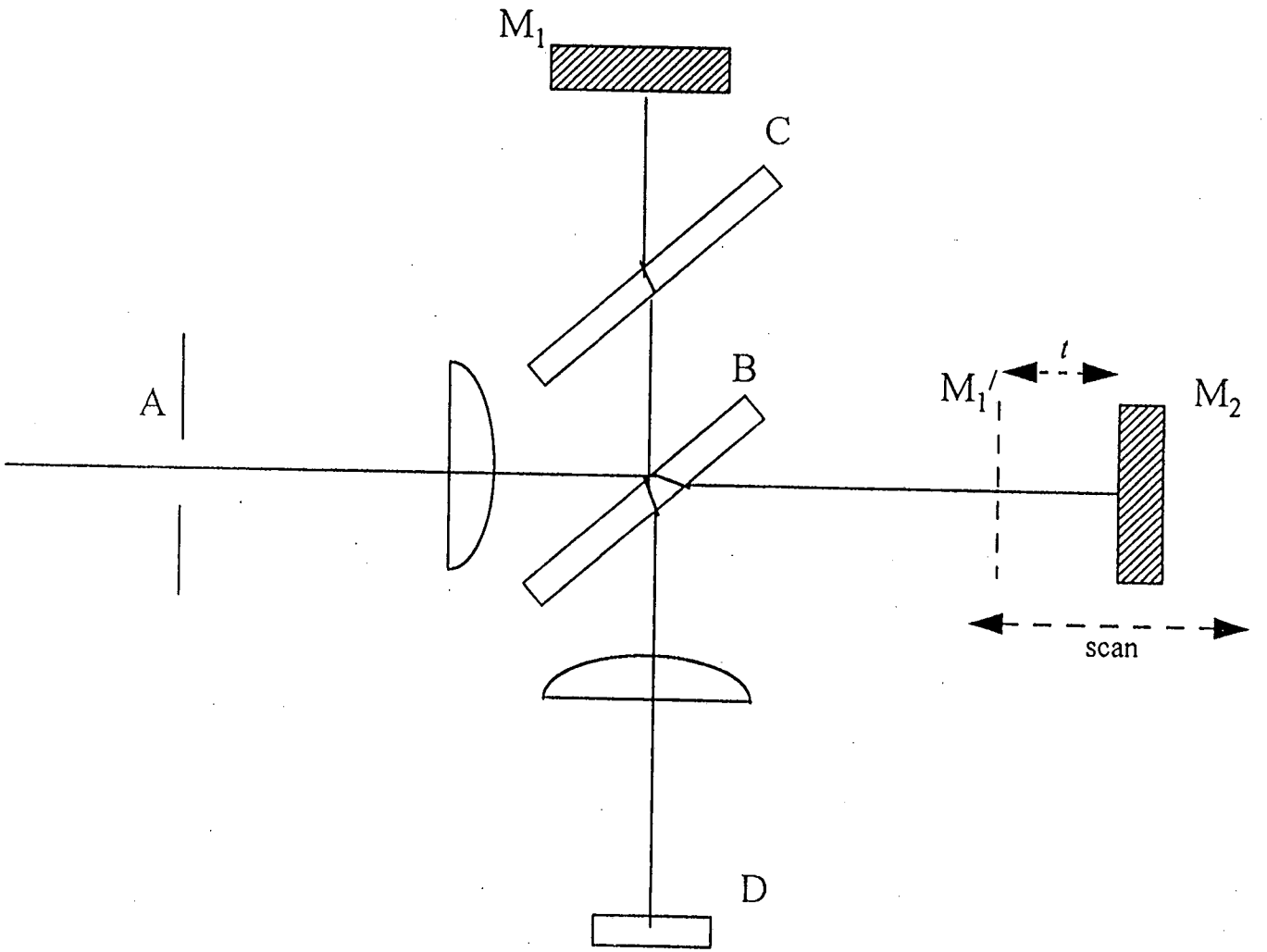

Figure 6

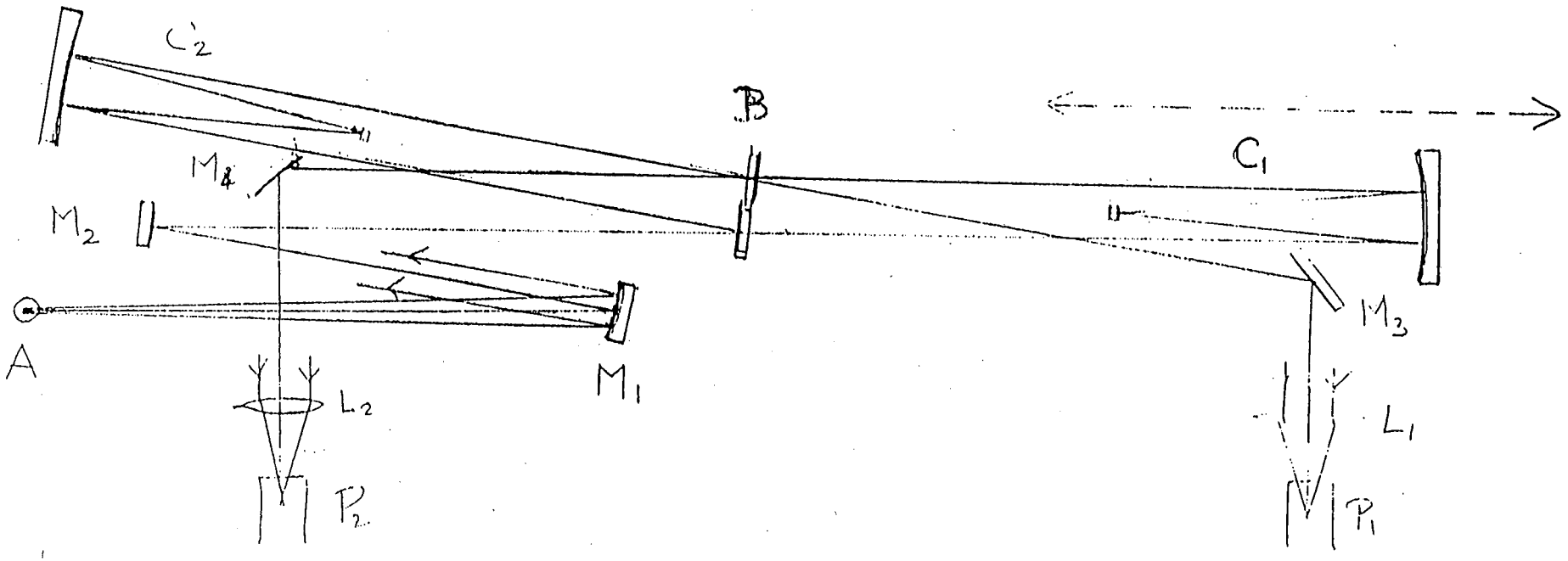

Figure 7

20 mA Pt lamp; 0.06 cm^{-1} resolution

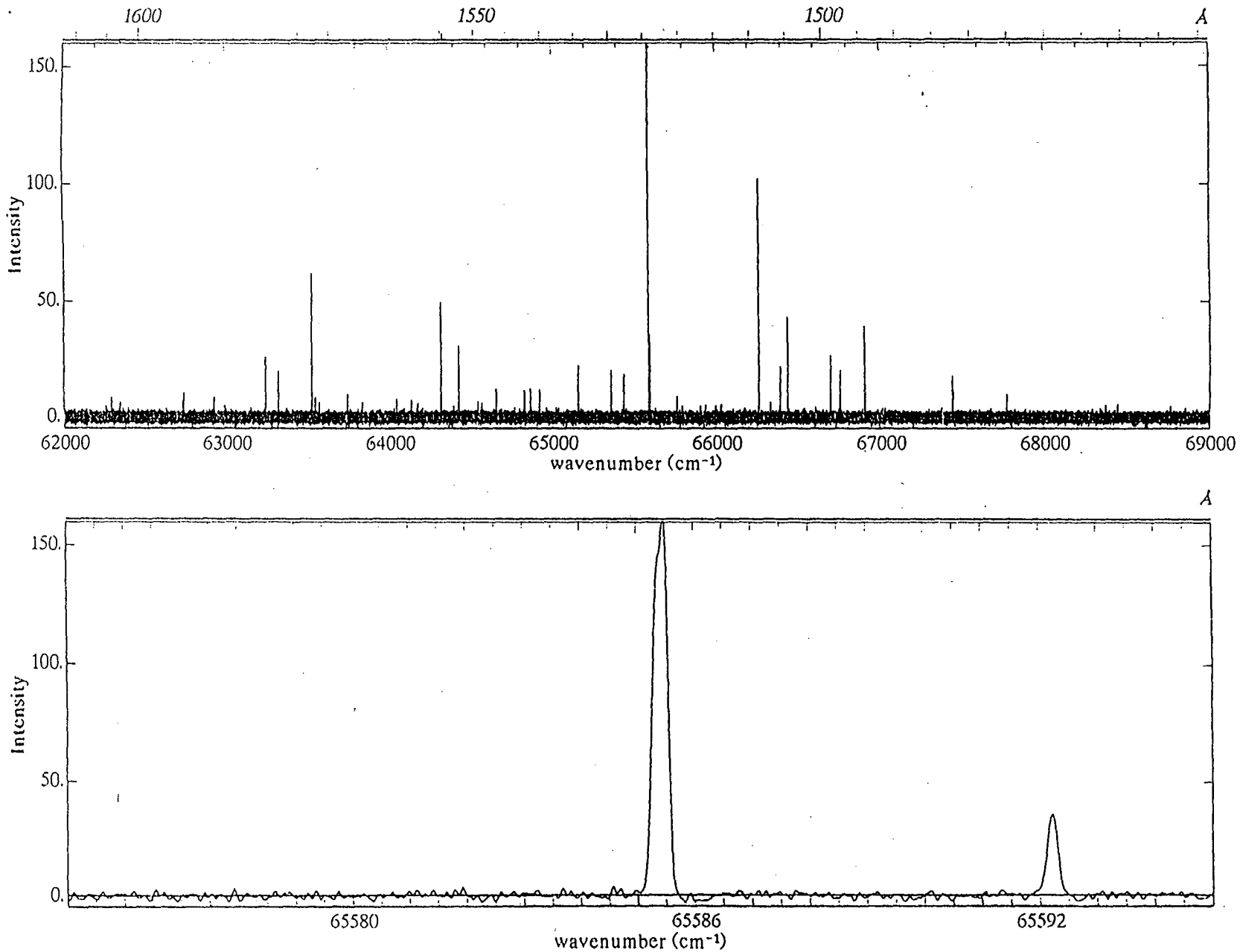

Figure 8

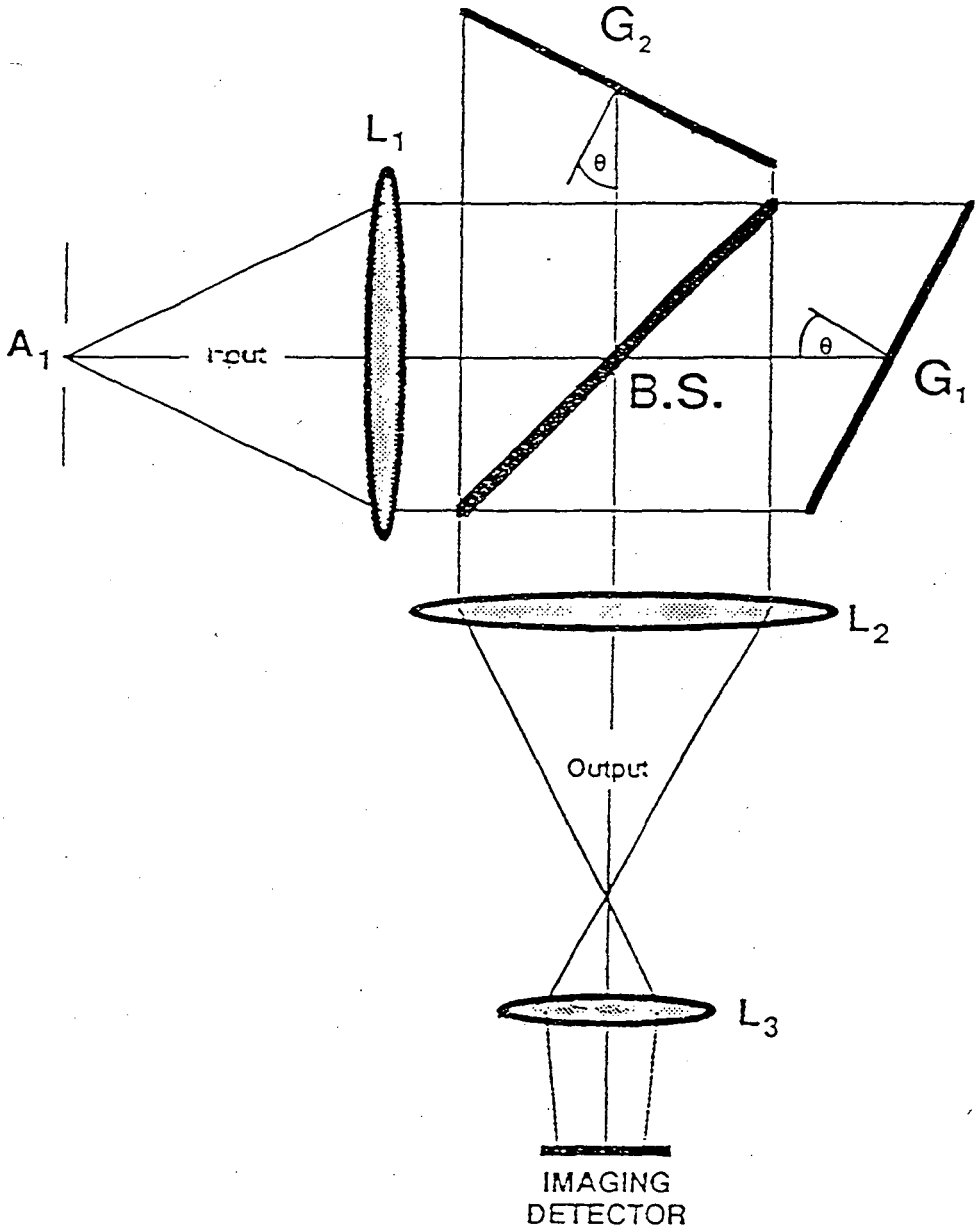

Figure 9

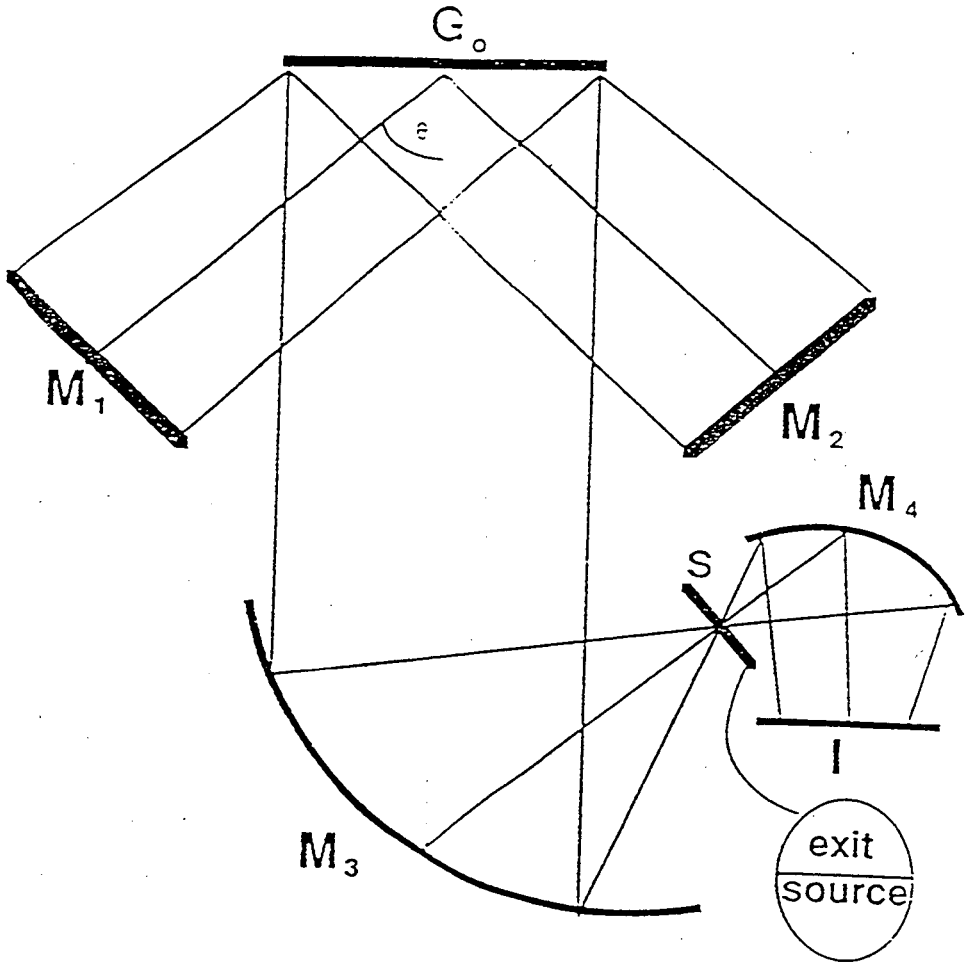

Figure 10

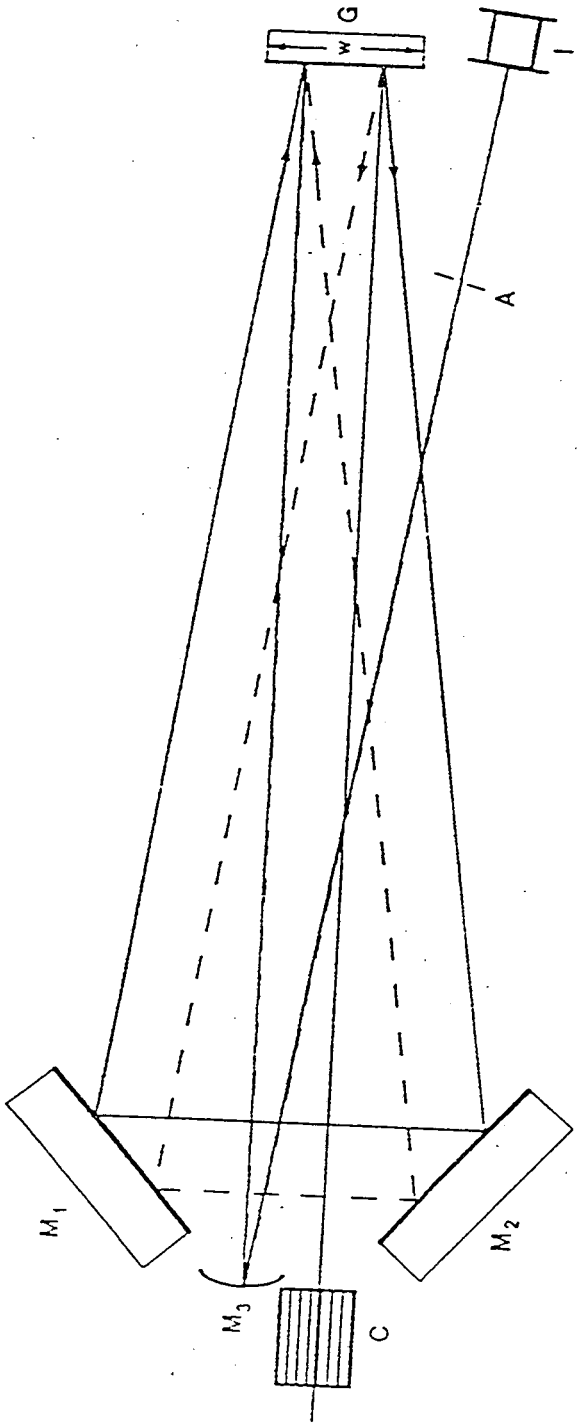

Figure 11

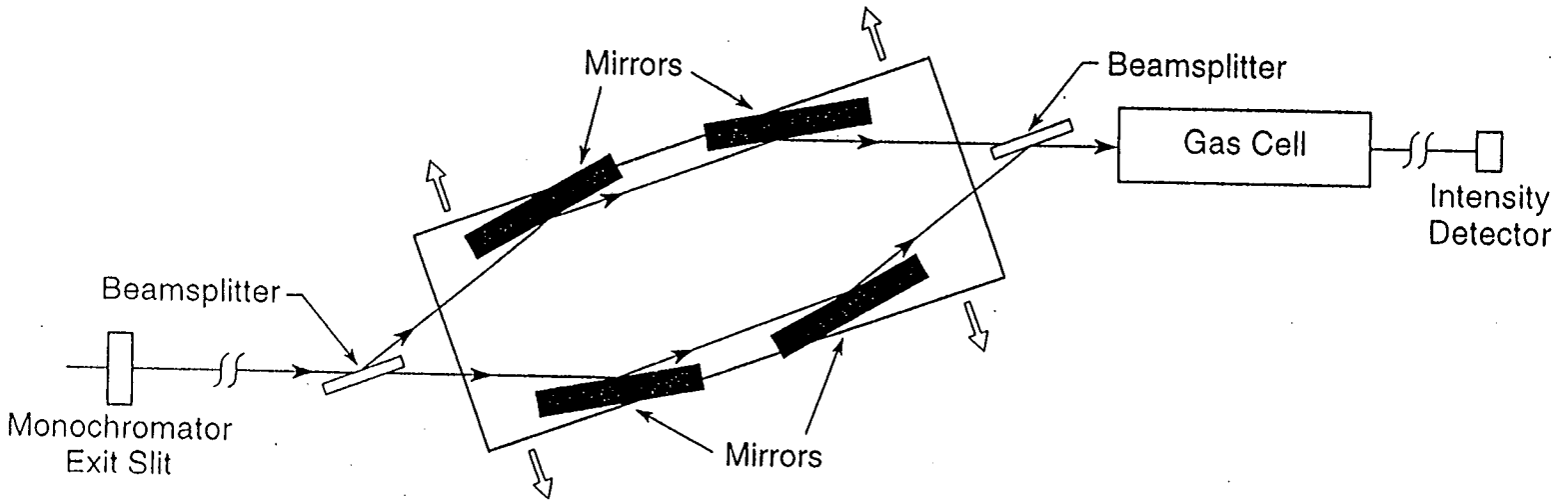
Mirrors
Beamsplitter
Gas Cell
Intensity
Detector
Beamsplitter
Monochromator
Exit Slit
Mirrors

Figure 12

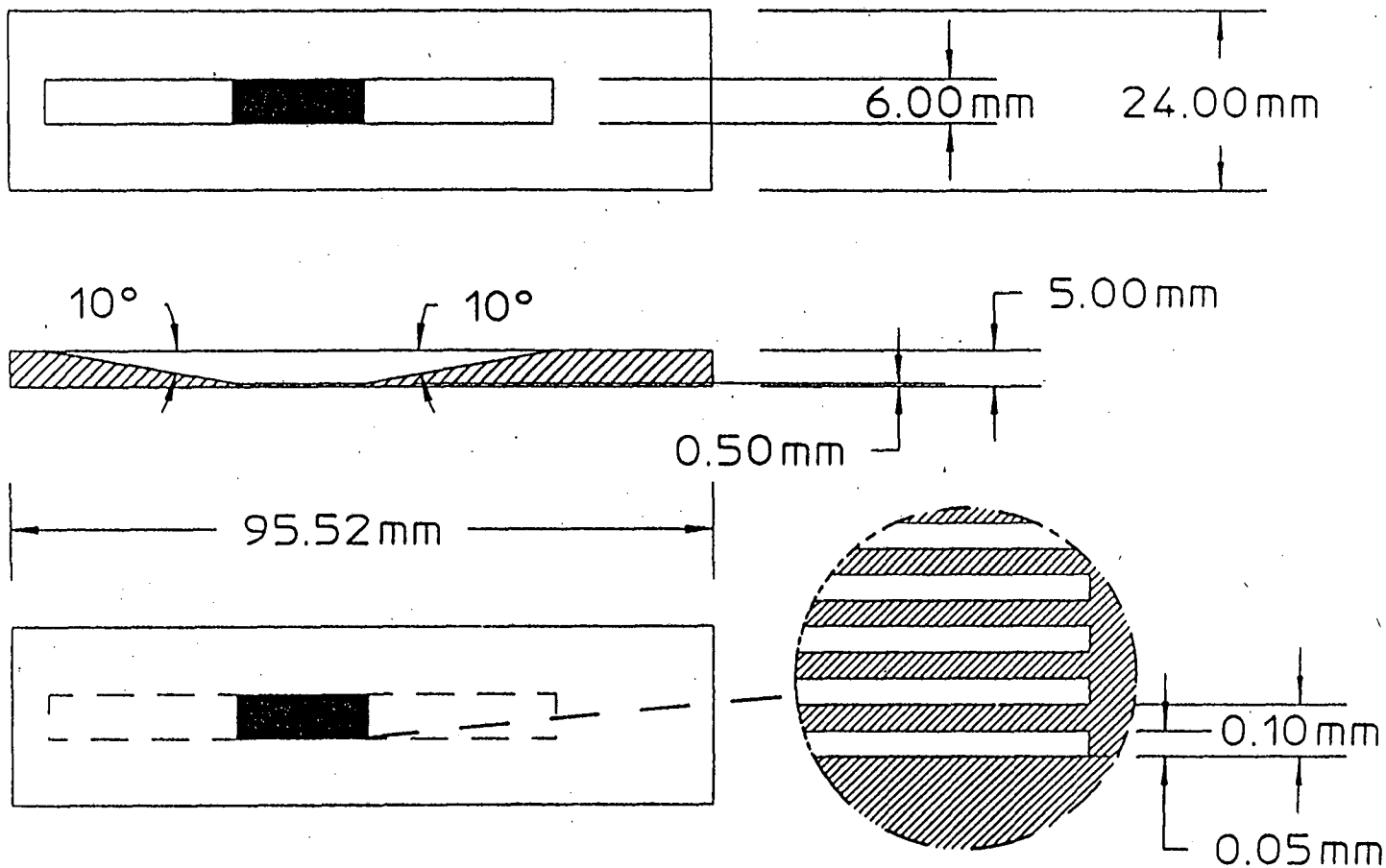

Figure 13

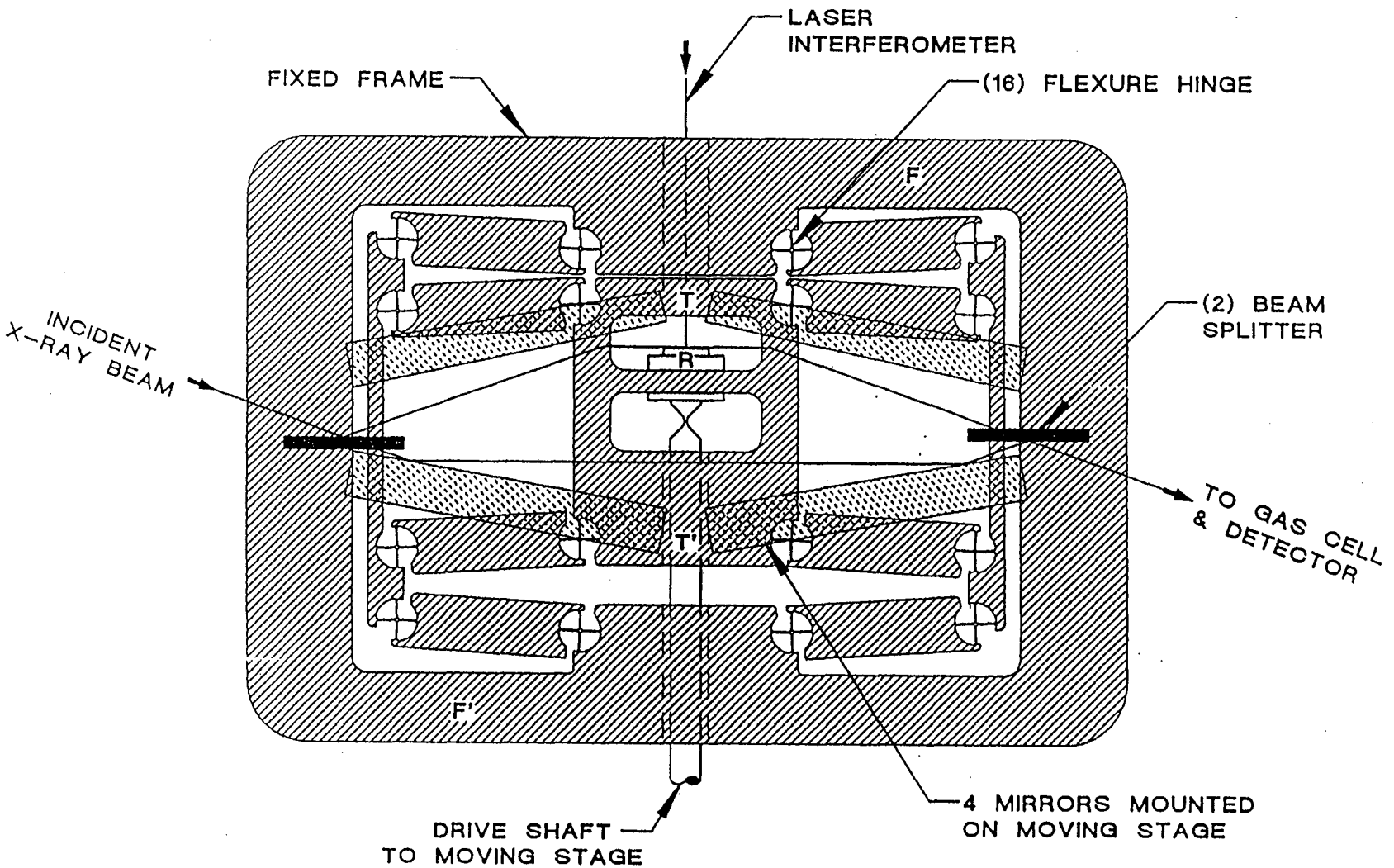
LASER
INTERFEROMETER
FIXED FRAME
(16) FLEXURE HINGE
F
T'
R
T'
F'
INCIDENT
X-RAY BEAM
(2) BEAM
SPLITTER
TO GAS CELL
& DETECTOR
4 MIRRORS MOUNTED
ON MOVING STAGE
DRIVE SHAFT
TO MOVING STAGE

Figure 14

Ernest Orlando Lawrence Berkeley National Laboratory
One Cyclotron Road | Berkeley, California 94720

Prepared for the U.S. Department of Energy under Contract No. DE-AC03-76SF00098